Improved evaporative flux partitioning and carbon flux in the land surface model JULES: impact on the simulation of land surface processes in temperate Europe

Agricultural and Forest Meteorology 181 (2013) 108–124

Contents lists available at ScienceDirect

Agricultural and Forest Meteorology

journal homepage: www.elsevier.com/locate/agrformet

Improved evaporative flux partitioning and carbon flux in the land surface model JULES: Impact on the simulation of land surface processes in temperate Europe

Catherine Van den Hoof[a,*], Pier Luigi Vidale[a], Anne Verhoef[b], Caroline Vincke[c]

[a] Department of Meteorology, The University of Reading, Earley Gate, PO Box 243, Reading RG6 6BB, United Kingdom
[b] Department of Geography and Environmental Science, The University of Reading, Whiteknights, PO Box 233, Reading RG6 6DW, United Kingdom
[c] Earth and Life Institute, Université catholique de Louvain (UCL), Croix du Sud 2, L7.05.09, B-1348 Louvain-la-Neuve, Belgium

ARTICLE INFO

Article history:
Received 26 November 2012
Received in revised form 20 July 2013
Accepted 23 July 2013

Keywords:
Eddy fluxes measurements
Europe
Evaporative flux partitioning
Land surface model
2003 heat wave

ABSTRACT

The primary role of land surface models embedded in climate models is to partition surface available energy into upwards, radiative, sensible and latent heat fluxes. Partitioning of evapotranspiration, ET, is of fundamental importance: as a major component of the total surface latent heat flux, ET affects the simulated surface water balance, and related energy balance, and consequently the feedbacks with the atmosphere. In this context it is also crucial to credibly represent the CO_2 exchange between ecosystems and their environment. In this study, JULES, the land surface model used in UK weather and climate models, has been evaluated for temperate Europe. Compared to eddy covariance flux measurements, the CO_2 uptake by the ecosystem is underestimated and the ET overestimated. In addition, the contribution to ET from soil and intercepted water evaporation far outweighs the contribution of plant transpiration. To alleviate these biases, adaptations have been implemented in JULES, based on key literature references. These adaptations have improved the simulation of the spatio-temporal variability of the fluxes and the accuracy of the simulated GPP and ET, including its partitioning. This resulted in a shift of the seasonal soil moisture cycle. These adaptations are expected to increase the fidelity of climate simulations over Europe. Finally, the extreme summer of 2003 was used as evaluation benchmark for the use of the model in climate change studies. The improved model captures the impact of the 2003 drought on the carbon assimilation and the water use efficiency of the plants. It, however, underestimates the 2003 GPP anomalies. The simulations showed that a reduction of evaporation from the interception and soil reservoirs, albeit not of transpiration, largely explained the good correlation between the carbon and the water fluxes anomalies that was observed during 2003. This demonstrates the importance of being able to discriminate the response of individual component of the ET flux to environmental forcing.

1. Introduction

The increasing demand for ecosystem services, in conjunction with climate change, are expected to significantly alter the terrestrial ecosystems and, by consequence, the energy, water, and carbon fluxes between land and atmosphere (Foley et al., 2005). In order to evaluate the sustainability of the ecosystems and their services, in particular future water availability, there is a need for a better understanding of the relationships between the land surface characteristics, and the energy and water cycles.

Simulating the various processes that interact within the hydrological cycle is a challenging task for climate models. Successful simulation of these interactions by the land surface component of a climate model requires detailed representation of processes such as interception, throughfall, snow accumulation, infiltration, runoff, soil moisture recharge and uptake, as well as the partitioning of evapotranspiration between intercepted water evaporation (from canopy and standing water on top of soil), transpiration, and soil evaporation (Oleson et al., 2008).

One of the primary roles of a land surface scheme in a General Circulation Model (GCM) is to partition net incoming radiation into upwards flux of long wave radiation, sensible heat (SH) and latent heat flux (LE), as well as downwards ground flux. In the absence of freeze/melt processes, the latent heat flux is directly proportional to total evapotranspiration (ET), i.e. the sum of transpiration (E_t), soil evaporation (E_s) and intercepted water evaporation (E_c). Since the time scales of response differ for each ET component (fast for E_c, slower for E_s, and slowest for E_t), the timescale of ET response and the local climate response, such as to a rainfall event or a seasonal precipitation anomaly, is likely to be affected by how the land

* Corresponding author.
E-mail address: catherine.vandenhoof@gmail.com (C. Van den Hoof).

0168-1923
http://dx.doi.org/10.1016/j.agrformet.2013.07.011

surface model in the GCM executes the partitioning. An underestimation of the role of E_t may also affect the amplitude and regionality of the land–atmosphere coupling in GCMs (Lawrence et al., 2006; Seneviratne et al., 2006), which has been used to assess the skill of models in predicting heat waves (Fischer et al., 2007).

Ecosystems are considered an important regulator of global climate. Plant transpiration generally decreases during dry and warm seasons, generally occurring in summer, due to lack of soil moisture supply. Subsurface hydrological processes on which these plants largely depend therefore need to be properly represented in land surface models in order to simulate the water and carbon cycles (Reichstein et al., 2002). With regards to climate change, model simulations indicate that extraordinary hot summers over North America, Central Asia, Europe and other mid-latitudinal regions will become more frequent, more intense and longer lasting in the future (Meehl and Tebaldi, 2004). From a modelling point of view the 2003 heat wave can be regarded as a proxy of future climate (Schär et al., 2004), so that demonstrated skill in simulating the chain of mechanisms active during summer 2003 is increasingly a key requirement for establishing the credibility of these prognostic tools. Analysis of extreme climatic events such as the 2003 heat wave and drought can improve our knowledge of the possible effect of climate change on the functioning of the ecosystem. It is important to credibly represent these processes, as they are crucially involved in feedbacks with the rest of the climate system. FLUXNET eddy-covariance data indicated a drop of 30% in GPP, Gross Primary Productivity, over Europe compared to 2002 (Ciais et al., 2005). This GPP drop coincided with a reduced evapotranspiration and soil drying due to the rainfall deficit (Reichstein et al., 2007). Hence, a successful modelling of the short-term effects on the carbon and water of the terrestrial ecosystem is a necessary condition for building confidence in future model predictions.

For this purpose, land surface models are useful tools. Examples of currently used land surface schemes include the Interaction Soil-Biosphere-Atmosphere model (ISBA, Noilhan and Planton, 1989), the Canadian Land Surface Scheme (CLASS, Verseghy et al., 1993), and the Community Land Model (CLM, Oleson et al., 2010). These models differ by their parametrisation and processes representation. A range of studies have investigated those differences as well as compared the simulated land surface fluxes and state variables that those models produce (Boone et al., 2004; Dirmeyer, 2011).

In this study, JULES, the Joint UK Land Environment Simulator (Clark et al., 2011; Best et al., 2011), which is the land surface model used in the weather, seasonal and climate models of the UK Met Office, will be evaluated for temperate Europe. JULES has been shown to improve the simulation of global surface climate when included in the HadAM3 version of the Hadley Centre climate model (Cox et al., 1999). However in comparison to all other AGCMs, Atmospheric General Circulation Models, considered in the GLACE project (Koster et al., 2006), the coupling strength between land and atmosphere in HadAM3 was among the weakest. The values for the ET coupling are low, when compared to other models for most regions of the world, including Europe. These low values may be due in part to unconstrained re-evaporation of canopy interception. They may also be due to the fact that evaporation in the HadAM3 model is rarely moisture-limited (Gedney et al., 2000). Blyth et al. (2010), who used surface energy flux measurements from 10 FLUXNET sites selected to represent a range of climate conditions and biome types worldwide to assess the performance of the land surface model JULES, found that in general LE is overestimated in JULES. The same results were found by Van den Hoof et al. (2011) over cropland in Europe. In addition to this, the simulated ET flux tends to fall too quickly during extended dry periods (Blyth et al., 2010), indicative of a source of moisture from small, unconstrained reservoirs. These results are consistent with what was found more recently during the assessment of the current Hadley Centre foundation for Earth System Modelling, HadGEM2 (Martin et al., 2010).

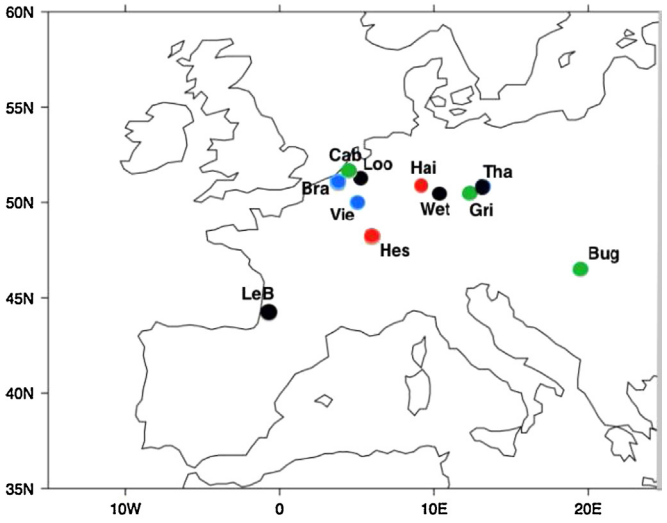

Fig. 1. Location of the needle leaf (black), broad leaf (red), mixed temperate (blue) forest and grassland (green) FLUXNET sites selected for this study. Site name abbreviations are explained in Table 1. (For interpretation of the references to colour in this figure legend, the reader is referred to the web version of the article.)

In this study, particular attention will be paid to the different components of ET and to the impact of their partitioning on the land surface state. JULES model output has mainly been evaluated against eddy covariance flux measurements from the FLUXNET network, which provided spatio-temporal information of energy, water and carbon fluxes at timescales which are relevant to climate simulations. Despite the few available detailed measurements on flux partitioning, an attempt will be made to understand the JULES model's shortcomings. In addition, adaptations, based on key literature references, to address specific deficiencies in JULES, will be implemented and evaluated. The observed and simulated variables for 2003 will be used as a benchmark to understand the performance of the model to simulate the impact of an extreme event on the land surface and its ecosystem.

2. Materials

2.1. FLUXNET site data

For this study, eleven FLUXNET sites were selected; eight forest sites and 3 grassland sites. The forest sites consist of two deciduous broadleaf (Hesse in France and Hainich in Germany), 4 evergreen needle leaf (Le Bray in France, Loobos in The Netherlands, and Tharandt and Wetzstein in Germany) and 2 mixed deciduous and evergreen forest sites (Vielsalm and Brasschaat in Belgium). The three grassland sites are Bugac (Hungary), Cabauw (The Netherlands) and Grillenburg (Germany). The locations of these sites are shown in Fig. 1. A summary of the key climatic and ecological conditions found at these FLUXNET sites is given in Table 1.

The sites were selected in such a way that they cover a wide range of temperate ecosystems in Western Europe. In addition to this, the data needed to span several years (>5 years) and by preference include 2003, during which a heat and drought wave was observed in Europe. The data availability for each site is provided in Table 1.

At all sites, the exchanges of carbon dioxide (CO_2), water vapour and energy were measured above the canopy using the eddy covariance method (Aubinet et al., 2000) at half-hourly time-steps. The monthly averaged fluxes of energy and water as well as the

Table 1
Summary of ecological, climatic, and soil characteristics at the temperate forest and grassland FLUXNET sites selected for this study.

	Location		Elev. (m)	Climate		Soil texture[a]	Landcover	H (m)	References	Years of data
	Lat (°)	Lon (°)		T(°C)	P(mm)					
Brasschaat (Bra)	51.18	4.31	16	11.1	824	Moderate wet loamy sand, haplic podzol (*coarse)	50% BL with LAI: 0–3.0 and h: 17 m 50% NL with LAI: 1.8 and h: 21 m	41	Gond et al. (1999), Carrara et al. (2003), Curiel Yuste et al. (2005), Gielen et al. (2010)	2000–2009 (except 2003)
Bugac (Bug)	46.69	19.6	114	10.4	562	Sandy loam (capillary rise), chernozem (*coarse)	100% grass with LAI: 1.5 and h: 0.5 m	4	Nagy et al. (2011), Balogh et al. (2011), Gilmanov et al. (2007), Flechard et al. (2011)	2003–2008
Cabauw (Cab)	51.97	4.93	−0.7	9.8	786	Alluvial clay on peat (*very fine)	100% grass with LAI: 2.0 and h: 0.2 m	10	Tolk et al. (2009), Gilmanov et al. (2007), Flechard et al. (2011)	2003–2008
Grillenburg (Gri)	50.95	13.51	385	7.2	853	Silt loam, pseudo-gley (*very fine)	100% grass with LAI: 3.5 and h: 0.7 m	3	Hussain et al. (2011), Prescher et al. (2010), Gilmanov et al. (2007), Flechard et al. (2011)	2004–2008
Hainich (Hai)	51.04	10.27	440	7.5	750	Chromic cambisol (*fine)	100% BL with LAI: 0–6 and h: 33 m	43.5	Knohl et al. (2003)	2000–2007
Hesse (Hes)	48.67	7.07	300	9.2	820	Loamy, (stagnic) luvisol (*medium fine)	100% BL with LAI: 0.5–5.5 and h: 16 m	22	Granier et al. (2000a), Granier et al. (2000b), Betsch et al. (2011)	2003–2008
Le Bray (LeB)	44.42	0.46	60	12.5	930	Sandy (*coarse)	100% NL with LAI: 1.8–4.2 and h: 18 m	25	Berbigier et al. (2001), Rivalland et al. (2005)	2000–2008
Loobos (Loo)	52.10	05.44	15.1	10.0	786	Sandy, humus podzol (*coarse)	100% NL with LAI: 2.3 and h: 16 m	26	Dolman et al. (2002)	2000–2009
Tharandt (Tha)	50.57	13.34	380	7.8	823	Loamy podzol, distric cambisol (*medium)	87% NL with LAI: 7.6 and h: 26.5 13% BL	42	Grünwald and Bernhofer (2007), Clausnitzer et al. (2011)	2000–2009
Vielsalm (Vie)	51.31	4.52	450	7.5	1000	Silt loam, distric cambisol (*medium)	60% BL LAI: 1–5 and h: 27 m 40% NL with LAI: 5.5 h: 35 m	40	Laitat et al. (1999), Aubinet et al. (2001), Aubinet et al. (2002)	2000–2009
Wetzstein (Wet)	50.27	11.27	450	7.5	1000	Silty clay, chernozem (*medium fine)	100% NL with LAI: 4 and h: 22	30	Anthoni et al. (2004), Rebmann et al. (2010)	2003–2008

T: mean annual air temperature, P: cumulated annual precipitation, h: height of vegetation, LAI: leaf area index and H: height of eddy flux measurements (max. values in case of grass), BL: broad leaf tree, NL: needle leaf tree.
[a] See Table 3 of Wösten et al. (1999).

carbon exchanges have been used to evaluate the variables simulated by the land surface model JULES. The FLUXNET data sets also provided all the meteorological variables required to force the model at half-hourly time-steps: global and net radiation (R_g and R_n), air temperature (T), specific humidity (q), precipitation and snow (P and S_n), wind speed ($|v|$) and surface pressure (p).

Based on site specific information provided for each site (see Table 1), the soils of the FLUXNET sites were allocated to one of the 11 possible soil textural/pedological classes derived from six FAO texture classes (five mineral and one organic) and two pedological classes (topsoil and subsoil), as described in Table 3 of Wösten et al. (1999). Wösten et al. (1999) assigned parameters, relating to curves describing the relationship of matric potential and hydraulic conductivity with moisture content (van Genuchten, 1980), to each of these soil classes. Those parameters were derived from a set of standardised pedotransfer functions applicable to studies at a European scale and can be found in Table 4 of Wösten et al. (1999).

2.2. The land surface model JULES v.2.2

JULES, the Joint UK Land Environment Simulator (Clark et al., 2011; Best et al., 2011) is the UK community land surface model. It was originally designed to represent the land surface in UK weather, seasonal and climate models, including all Hadley Centre climate models, but has been increasingly used as a community model for more general purposes such as impact studies (Betts, 2007; Harrison et al., 2008).

JULES calculates surface prognostics of temperature, specific humidity and snow cover, as well as the fluxes of moisture, CO_2, momentum and energy between the land surface and the atmosphere. The surface fluxes of moisture and heat are functions of the atmospheric driving variables: T, q, p, $|v|$, R_n (and R_g), $P+S_n$. Evaporation from the surface comes from three sources: there is the evaporation from interception storage (at potential rate), bare soil evaporation from the top soil layer, and transpiration originating from root water uptake from all four model layers over vegetated areas.

JULES uses a tiled model of sub-grid heterogeneity with separate surface temperatures, short-wave and long-wave upwelling radiative fluxes, sensible and latent heat fluxes, ground heat fluxes, canopy moisture content, snow mass and snow melt. JULES uses five vegetation tiles, representing five different Plant Functional Types (PFTs: broad-leaf trees, needle-leaf trees, C3-grass, C4-grass, shrubs) and four non-vegetated surface tiles (urban, inland water, bare soil and ice). These five PFTs differ in their morphological, physiological and hydrological characteristics.

The soil consists of four layers extending to 3 m depth. The layers have a thickness of 0.1 m, 0.25 m, 0.65 m and 2 m, respectively. These 4 soil layers have specific hydraulic and thermodynamic properties. Movement of water through the soil is calculated via the Richards equation, and hydraulic conductivity and pressure head are calculated using Clapp and Hornberger (1978) or van Genuchten (1980) characteristic curves, see Eq. (13). Precipitation falls on the surface; a fraction is intercepted by the canopy with the remainder falling to the surface as throughfall. The water reaching the soil surface is then split between infiltration into the soil and surface runoff. The infiltration takes place at a rate equal to the saturated hydraulic conductivity multiplied by an infiltration enhancement factor, which is dependent on the presence and type of vegetation. From the deepest soil layer, drainage takes

place at a rate equal to the hydraulic conductivity of this layer ('free drainage').

Further details on the JULES model formulation, directly relevant to the moisture flux, are described in the following section. A more detailed description of the model can be found in Clark et al. (2011) and Best et al. (2011).

3. Methods

3.1. Summary of model improvements

In this section, the modifications that were implemented in JULES v.2.2 to better represent the different components of the moisture flux are described. These modifications are based on key literature references; no model tuning was performed.

3.1.1. Vegetation transpiration

Transpiration depends on the net radiation, the bulk transfer coefficient for heat and water vapour, the vapour pressure deficit of the air, the leaf area index and the stomatal resistance. In JULES this stomatal conductance is represented by the $A-g_s$ scheme developed by Jacobs (1994):

$$g_s = \left(\frac{1.6RT_*}{C_c - C_i}\right) A \tag{1}$$

$$C_i = \left[f_0\left(1 - \frac{D_*}{D_c}\right)(C_c - \Gamma)\right] + \Gamma \tag{2}$$

with g_s the stomatal conductance to water vapour ($m\,s^{-1}$), R the universal gas constant ($J\,K^{-1}\,mol^{-1}$), T_* the leaf surface temperature (K) and A the net photosynthetic rate ($mol\,CO_2\,m^{-2}\,s^{-1}$). The factor 1.6 accounts for the different molecular diffusivities of water and carbon dioxide. C_i the internal CO_2 partial pressure (Pa) is a function of C_c the leaf surface CO_2 partial pressure (Pa), Γ the photorespiration compensation point (Pa), D_* the specific humidity deficit at the leaf surface ($kg\,H_2O\,kg^{-1}$ air), D_c the critical humidity deficit ($kg\,H_2O\,kg^{-1}$ air) and f_0 the maximum ratio between intercellular and atmospheric CO_2. f_0 (dimensionless) is defined as C_i/C_c for $D_* = 0$. Based on the simplified formulation by Leuning (1995), values can be assigned to f_0 and D_c:

$$f_0 = 1 - \frac{1.6}{a} \tag{3}$$

$$D_c = \left(\frac{a}{1.6} - 1\right) D_0 \tag{4}$$

with a, a dimensionless parameter, and D_0 equal to 6.23 and 0.0281 $g\,kg^{-1}$, respectively.

The leaf photosynthesis A depends on a number j of environmental variables X (water availability, net radiation, temperature) as well as the internal CO_2 concentration, C_i:

$$A = A(X_j, C_i) \tag{5}$$

JULES uses a biochemical approach to estimate the non water- and nutrient-limited photosynthesis. It is based on the model of Collatz et al. (1991) for C3-type photosynthesis and Collatz et al. (1992) for C4-type photosynthesis. These models describe the rate of CO_2 assimilation as limited by enzyme kinematics: (i) the amount of Rubisco; (ii) the electron transport, which is a function of available light and (iii) the capacity to transport or utilise photosynthetic products. (i) and (iii) are a function of the maximum rate of carboxylation of Rubisco, V_m. In JULES, V_m is a function of V_{max} the maximum rate at 25 °C and T^*. V_{max} depends on the leaf nitrogen concentration n_l, which is kept constant per PFT:

$$V_{max} = \begin{cases} 0.0008\,n_l & \text{for } C_3 \\ 0.0004 n_l & \text{for } C_4 \end{cases} \tag{6}$$

Finally, the leaf photosynthetic rate is up-scaled to the canopy level by means of the leaf area index, LAI.

Cox et al. (1998) have treated the parameters n_l, D_c and f_0 of JULES as calibration parameters. By least squares optimisation of the model, they assigned to these parameters the values provided in Table 2 and currently used by Clark et al. (2011). In this study we propose new values, guided by plant physiology literature and the leaf stomatal conductance formulation used in JULES and developed by Leuning (1995).

In his review on biochemical limitations to carbon assimilation in C_3 plants, Wullschleger (1993) provided average values for measured maximum rate of carboxylation per PFT. The values provided in Table 2 for n_l per PFTs are interpolated from these rates based on Eq. (6). However, Wullschleger (1993) mentioned that in the case of conifers some artefact may be present that causes a bias in the estimates of the maximum rate of carboxylation; i.e. the temperatures used to define this rate for many of the conifer species were lower than those used for other plant species.

Next, Reich et al. (1995) suggested that conifer high instantaneous photosynthetic nitrogen use efficiency, rather than leaf nitrogen concentration per se, plays an important role in the response of the maximum photosynthetic rate to variation in leaf nitrogen. The use of n_l to estimate the maximum rate for evergreen trees might lead to underestimation. Furthermore, Gibelin et al. (2006) mentioned that leaf structure is more relevant to maximum photosynthetic rate than leaf nitrogen. Therefore in the flux modelling study performed at high and middle latitude (Gibelin et al., 2008), the value of n_l for needle leaf tree was set to 0.07 $kgN\,kg^{-1}$ C, instead of 0.031 $kgN\,kg^{-1}$ C as extrapolated from the study by Wullschleger (1993).

Concerning D_c and f_0, based on Eqs. (3) and (4), the values corresponding to these parameters are 0.081 $kg\,kg^{-1}$ for D_c and of 0.74 (dimensionless) for f_0. These values are in agreement with the experimental results given by Goudriaan and Van Laar (1978) and Wong et al. (1979).

Based on the literature review above, the value of n_l for needle leaf trees was changed in our study to 0.07; this is a doubling of the value compared to the value provided by Clark et al. (2011). The values for the other vegetation types, broad leaf tree and C3-grass were not adapted. D_c and f_0 were changed to 0.081 and 0.74, respectively, for all vegetation types. This means that for broad leaf tree and C3-grass, D_c decreased by 10% and 19%, respectively, compared to Clark et al. (2011). The value for needle leaf trees increased by 35%. Concerning f_0, its value was reduced for all vegetation types compared to Clark et al. (2011); by 15% for the trees and by 18% for the C3-grass. These proposed new values are given in Table 2.

Finally, based on the literature review performed by Breuer et al. (2003) for land covers in temperate ecosystems, the

Table 2
Values of n_l ($kgN\,kg^{-1}$ C), D_c ($kg\,H_2O\,kg^{-1}$ air) and f_0 (dimensionless) for broad leaf trees (BL), needle leaf trees (NL) and C3-grass, as used in the literature as well as those selected for this study (proposed values). The values currently used in JULES (JULES-orig) are represented in bold.

	Wullschleger (1993)	Clark et al. (2011)			Proposed values		
	n_l	n_l	D_c	f_0	n_l	D_c	f_0
BL	0.059	**0.046**	**0.090**	**0.875**	0.046	0.081	0.74
NL	0.031	**0.033**	**0.060**	**0.875**	0.07	0.081	0.74
C_3-grass	0.075	**0.073**	**0.100**	**0.900**	0.073	0.081	0.74

rooting depths of BL and NL were both set to 1.2 m, instead of 3 m and 1 m, respectively. BL and NL were not differentiated where rooting depth is concerned since the intra-species variability is larger than the inter-species variability. The value of 0.5 m for the rooting depth of grassland was left unchanged.

3.1.2. Intercepted water evaporation

The evaporation of intercepted water only takes place from the saturated fraction of the canopy, f_a. In JULES, f_a is defined as follows:

$$f_a = \frac{C}{C_m} \tag{7}$$

where C the canopy moisture content (in kg m^{-2}) and C_m the canopy capacity (in kg m^{-2}).

An alternative equation for Eq. (7) has been provided by Deardorff (1978):

$$f_a = \left(\frac{C}{C_m}\right)^{2/3} \tag{8}$$

This formulation is currently used in the CLM (Oleson et al., 2010) and in the land surface model ISBA (Noilhan and Lacarrère, 1995), and has been implemented in JULES in this study by replacing Eq. (7) with Eq. (8). This adaptation will result in a reduced saturated fraction and hence a larger dry land surface fraction $(1 - f_a)$. This means that a larger fraction of evaporation will come from vegetation transpiration and soil evaporation.

With regards to C_m, the canopy capacity, this is currently computed in standard JULES as:

$$C_m = 0.5 + 0.05\text{LAI} \tag{9}$$

The above formulation was compared to formulations used in other land surface models. The canopy moisture content C_m is defined by Sellers et al. (1996) and Dickinson et al. (1993) as equal to 0.1 LAI and by Tallaksen (1991) as 0.2 LAI. These values are in line with the literature review performed by Breuer et al. (2003) for various plant parameters in temperate climate. This review mentions a mean interception, which corresponds to C_m, of 1.8 (kg m^{-2}) for NL, 1.4 (kg m^{-2}) for BL and 1.5 (kg m^{-2}) for C3-grass, with a mean LAI value of 6.2, 5.8 and 7.2, respectively. Based on this, the formulation for the canopy capacity C_m (Eq. (9)) in JULES has been replaced with:

$$C_m = 0.05 + 0.2\text{LAI} \tag{10}$$

A minimum water interception of 0.05 kg m^{-2} has been chosen assuming that the soil, branches and trunk intercept water as well. This adaptation will result in an enhanced dependency of canopy interception to LAI.

3.1.3. Soil evaporation and infiltration

3.1.3.1. Soil evaporation. In JULES, the soil evaporation depends on the soil conductance (m s^{-1}), g_{soil}, which has been defined as follows:

$$g_{soil} = \frac{1}{100}\left(\frac{\theta_1}{\theta_c}\right)^2 \tag{11}$$

with θ_1 the volumetric soil moisture content (m^3 m^{-3}) in the top 0.1 m of the soil (layer 1) and θ_c the volumetric soil moisture content at critical point (=field capacity) within the same layer. Hence, the soil evaporation rate depends on the moisture content within the top 0.1 m. However, as mentioned by Mahfouf and Noilhan (1991), simple parameterisations of soil evaporation are only valid for a thin layer of a few centimetres. In CLM for example, the soil evaporation depends on the soil moisture content within the top 0.0175 m (Lawrence et al., 2006). Therefore we decided to reduce the depth of the top soil layer in JULES. The model however becomes numerically unstable if the top layer is less than about 0.025 m thick (also confirmed by personal communication with J. Edwards, UKMO – 22/11/2011). Therefore a different approach has been used in this study. The top soil layer evaporation capacity has been reduced to 0.0175 m; the top soil layer of 0.1 m is assumed to deplete gradually by evaporation only over the top 0.0175 m, whereas the transpiration for the first layer can take place over the entire top 0.1 m. This has been implemented in JULES by replacing Eq. (11) by the following equation:

$$g_{soil} = \begin{cases} \dfrac{1}{100}\left(\dfrac{\theta_1 - (8.25/10.0)\theta_{sat}}{\theta_c(1.75/10.0)}\right)^2 & \\ 10^{-6} & \text{if } \dfrac{8.25}{10.0}\theta_{sat} > \theta_1 \end{cases} \tag{12}$$

with θ_{sat} the volumetric soil moisture concentration at saturation. Once the top 0.0175 m of the soil is depleted, g_{soil} is set to a very small value, 10^{-6} m s^{-1}, to limit the soil evaporation.

3.1.3.2. Top soil layer texture. As the top soil layer in forests and grasslands is usually rich in organic matter (Lawrence and Slater, 2008), the hydraulic parameters of this layer have been assigned the values provided in Table 4 of Wösten et al. (1999) for the *organic* soil texture class. The available soil water content, which is defined as the volumetric water content between θ_w (wilting point) and θ_c, is larger for organic soils compared to the other soil texture classes. In addition to this, the saturated hydraulic conductivity for this soil type is very small. Only the '*medium fine*' texture class presents lower values.

3.1.3.3. Infiltration enhancement factor. In JULES the surface infiltration rate K is equal to βK_s. K_s is the soil saturated hydraulic conductivity and β is an enhancement factor. The infiltration enhancement factor is set to 4 for BL and NL and to 2 for C3-grass vegetation type (Essery et al., 2001). These values were originally set equal to 6 and 1.5, respectively (Cox et al., 1999). In this study, the difference in saturated hydraulic conductivity between top and sublayer is already taken into account by using the hydraulic parameters values provided by Wösten et al. (1999) for top and sublayer. Note that Thompson et al. (2010) found no significant difference in infiltration capacity between hardwood, pine forests and grass. Therefore, in this study, the value of the β factor was set to 1 for all PFTs since no universal justification can be found for differences in β values between PFTs.

3.2. Model simulations

Model simulations were performed for the different FLUXNET sites for the adapted model versions as well as for the original JULES model. For each simulation, JULES was parameterised according to the FLUXNET site specific conditions (see Table 1). Due to the lack of observed times series of LAI, the model was forced with prescribed seasonal LAI values (see Table 1 for references). The distance between canopy height and the zero-plane displacement height H-d, with d the displacement height, is a required parameter in JULES. The values for d were taken from site specific information for Brasschaat and Vielsalm: 19 m (Carrara et al., 2003) and 28.5 m (Ligne et al., 2010), respectively, or set to 2/3 h (Brutsaert, 1982) for the other sites.

JULES was run using the van Genuchten soil hydraulic model to describe the soil water retention curve. This is in line with current practice in operational NWP at the UK Met Office and in climate prediction since the advent of HadGEM3 (Walters et al., 2011). The values for the van Genuchten parameters θ_r, residual water content (m^3 m^{-3}), θ_s, saturated water content (m^3 m^{-3}), K_s, saturated

hydraulic conductivity ($m\,s^{-1}$), the fitting parameter α (m^{-1})) and the shape parameters of the water retention curve, m and n, have been taken from Wösten et al. (1999). Given the soil texture class observed at the sites, the top soil layer in JULES has been assigned the *'topsoils'* parameter values provide in Table 4 of Wösten et al. (1999). The values of the *'subsoils'* category in Table 4 of Wösten et al. (1999) have been assigned to the 3 sublayers of JULES. The values for θ_w and θ_c, the wilting (or field capacity) and critical point ($m^3\,m^{-3}$), respectively, have been computed as follows:

$$\theta = \theta_r + \frac{\theta_s - \theta_r}{(1 + (\alpha\psi)^n)^m} \quad (13)$$

with ψ the pressure head, set to 1.5 MPa for $\theta = \theta_w$ and to 0.033 MPa for $\theta = \theta_c$. The values, based on Wösten et al. (1999), of the different hydraulic parameters required by JULES are provided in Table A.2 of Appendix A.

JULES was forced with the half-hourly meteorological conditions observed at the FLUXNET sites. For each simulation, the model was spun up using a loop of the time series of available forcing data (see Table 1) to ensure that the deep soil water was at equilibrium before conducting the final simulation. Equilibrium state was assumed to be reached once the difference with initial conditions was less than 1% for soil moisture and temperature.

3.3. Model performance and impact of adaptations

The original, as well as the adapted JULES versions, were evaluated at the different FLUXNET sites. The original JULES, as described in Section 2.2, is called *JULES-orig*. The simulation performed with JULES adapted for the vegetation transpiration (see Section 3.1.1) is called *Veg-mod*. The simulation performed with JULES adapted for the intercepted water evaporation (see Section 3.1.2) is called *Inter-mod*. The simulation performed with JULES adapted for the soil evaporation and infiltration (see Section 3.1.3) is called *Soil-mod*. Finally, the simulation performed with JULES including all adaptations is called *JULES-adapt*.

At each site, the latent heat exchanges [$W\,m^{-2}$] and the GPP [$gC\,m^{-2}$] simulated at half-hourly timestep and integrated to daily totals were tested and validated against the FLUXNET data. The model performance has been quantified in several ways. The correlation coefficient, *r*, between measured and simulated values was used to evaluate how well the observations and simulations vary jointly. The mean bias errors, MBE, and the Root Mean Squared Error, RMSE, were calculated as well. The MBE calculations provide an estimate of whether the model has tendencies to over-predict (*i.e.*, positive bias) or to under-predict (*i.e.*, negative bias) the fluxes with respect to observations. The RMSE is a measure of the deviation between the model and the observations. The latter is used to quantify the accuracy of the simulations.

The simulations performed with the different adapted versions have been compared to the original version *JULES-orig*, which has been used as a reference. The impact of each modification has been assessed by quantifying the significance of the changes in GPP, evaporative fluxes and extractable water, which is defined as the volumetric soil moisture content between the actual water content and the critical point in the top 3 m of the soil. The analysis of the soil moisture distinguishes between the top soil layer (0–0.1 m) and the rest of the soil profile (0.1–3 m). The significance of the changes has been quantified by means of the *t*-test. In this study the confidence level has been set to 95%.

While the model is forced by design to obey energy balance closure, we acknowledge that the lack of closure of the measured energy balance at FLUXNET sites, as discussed by Twine et al. (2000) and Wilson et al. (2002), is an issue. The lack of closure can potentially be corrected by a method based on the Bowen ratio approach (Twine et al., 2000), which assumes that the available energy and the Bowen ratio measurements are sufficiently accurate. However, data on ground heat fluxes and heat storages in the canopy were only available for a few sites, and this will bias the quantification of the lack of closure. In addition to this, Baldocchi and Ryu (2011) mentioned that the lack of energy balance closure is not necessarily due to a lack of quality or accuracy of the evaporation measurements, and that there is a growing body of evidence showing good agreement between long-term evaporation measurements by eddy covariance with independent hydrologically based methods. Therefore, since the reasons for the lack of closure are still under discussion (Foken et al., 2011), we have decided not to perform the flux correction procedure.

Finally, it has to be reiterated that the FLUXNET GPP data are extrapolated, through modelling, from measurements of Net Ecosystem Exchange, NEE (Falge et al., 2002; Reichstein et al., 2005). This method might generates biases in the provided GPP FLUXNET data as well.

4. Results and discussion

4.1. Original JULES v2.2 simulations

The performance of *JULES-orig*, has been evaluated against the FLUXNET data. From Fig. 2(a) and (b) it can be seen that the biases between JULES and FLUXNET mean cumulative yearly gross assimilation (GPP) and evapotranspiration (ET) vary from one site to another. At all sites, however, the modelled ET is significantly larger than the FLUXNET data (see also mean and MBE values in Table 3), in particular at Bra, Gri, Hai, Hes and Vie. The modelled GPP, in contrast, is significantly smaller compared to FLUXNET, except at Cab, Hai and Hes. At Gri the GPP is largely overestimated. Overall the model does not seem able to capture the spatial variability of GPP and ET. The correlation between modelled and measured mean yearly fluxes per site is very poor (see *r* values in Table 3) and not significant ($p > 0.5$). Furthermore, the RMSE values for both correlations are much larger than the observed natural spatial variability, which has been approximated by the standard deviation of the yearly observed values (St. dev. in Table 3) over the period provided in Table 1. This observed natural heterogeneity is significantly larger than the modelled heterogeneity, in particular in the case of the evapotranspiration rate.

Concerning the inter-annual variability, the correlation between modelled and observed yearly anomalies with the mean GPP and ET at the different sites over the time series provided in Table 1 is weak. The correlation coefficient *r* is equal to 0.62 ($p < 0.0001$) and 0.46 ($p = 0.00013$), for GPP and ET, respectively. This means that the model does not capture well the inter-annual variability. At monthly times scales, the correlations between FLUXNET data and JULES simulations of GPP and ET are much stronger. The *r* values are equal to 0.91 and 0.85 ($p < 0.0001$), respectively. At this time scale, the RMSE is around half the observed and modelled seasonal variability.

In Fig. 3(a) and Table 4 the partitioning of the modelled yearly evapotranspiration flux between its different components is presented. Results show that the contribution of the transpiration, soil and intercepted water evaporation to the total evapotranspiration rate is not in line with what can be found in the literature. According to a global process-based study performed by Miralles et al. (2011), the transpiration accounts for 80% of the annual land evaporation, interception loss for 11%, bare soil evaporation for 7% and snow sublimation for 2%. More specifically for Europe, the interception loss represents 18%. A study by Choudhury and DiGirolamo (1998), based on 132 geographically distributed catchments, estimated the ratio of transpiration to evapotranspiration around 0.65–0.7 for

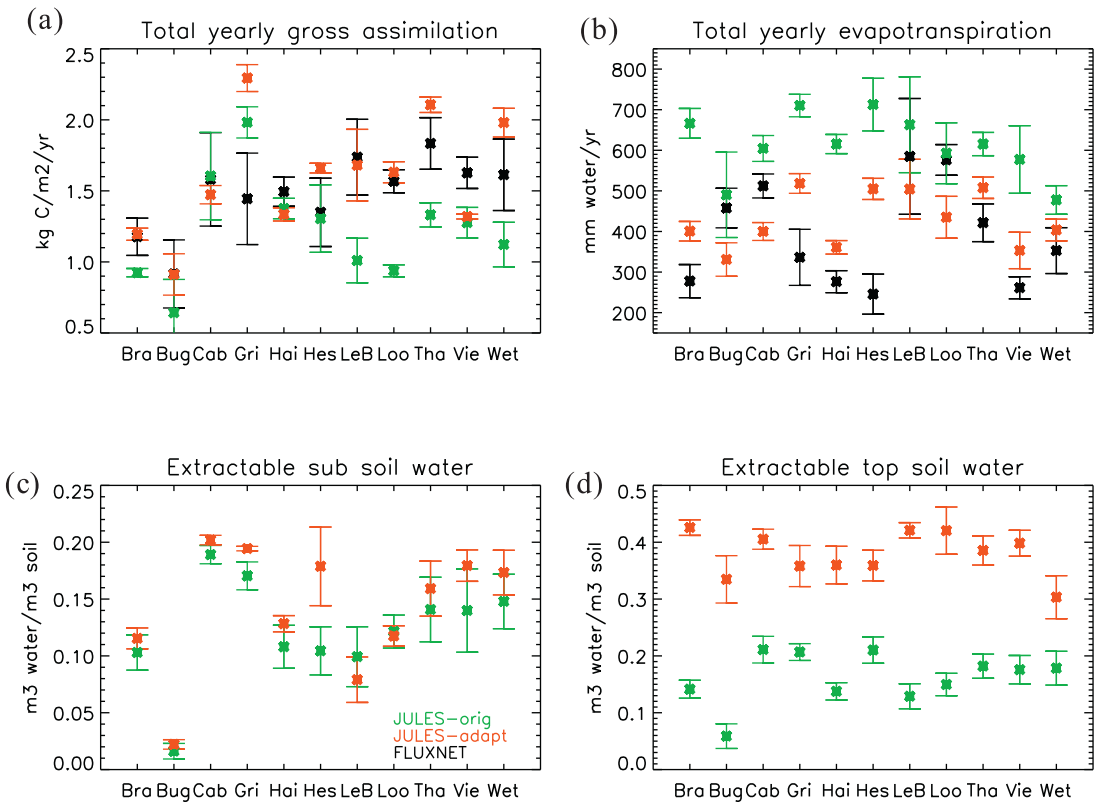

Fig. 2. Mean and standard deviation of the yearly gross assimilation (a), evapotranspiration (b), extractable soil water within 0.1–3 m (c) and with 0–0.1 m depth (d) at each site for the time series given in Table 1. The FLUXNET data are represented in black, the *JULES-orig* simulations in green and the *JULES-adapt* in red. (For interpretation of the references to colour in this figure legend, the reader is referred to the web version of the article.)

Table 3
Statistics for the mean yearly evapotranspiration (ET in mm year^{-1}) and gross assimilation (GPP in kg m^{-2} year^{-1}) at the selected sites simulated with the different JULES versions versus FLUXNET data.

	FLUXNET	Original	Veg-mod	Veg-mod + Inter-mod	Veg-mod + Soil-mod	Adapted
ET						
Mean	391.1	611.4	585.7	579	495.1	429.0
St. dev.	120.7	73.7	68.1	75.5	66.1	66.0
r	–	−0.20	0.25	−0.18	0.07	0.16
RMSE	–	268.5	230.0	243	169.1	133.5
MBE	–	220.2	194.6	188	104.0	37.9
GPP						
Mean	1.49	1.23	1.56	1.29	1.67	1.6
St. dev.	0.25	0.35	0.37	0.37	0.39	0.39
r	–	0.39	0.72	0.42	0.71	0.63
RMSE	–	0.43	0.27	0.40	0.33	0.33
MBE	–	−0.26	0.08	−0.19	0.19	0.11

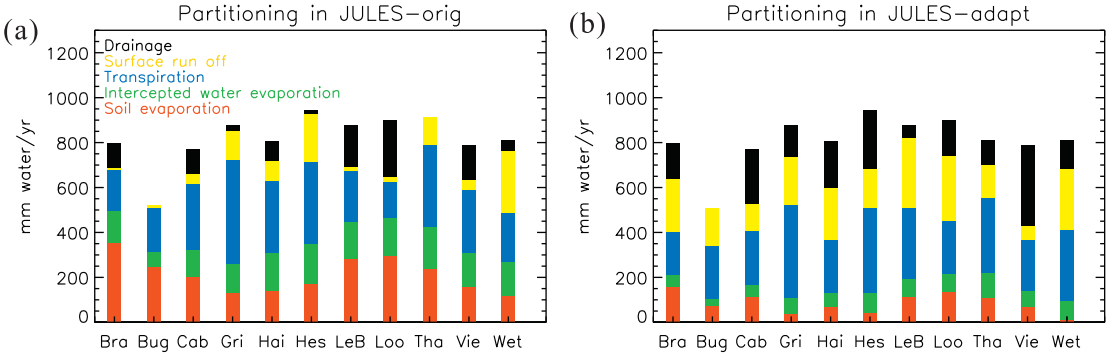

Fig. 3. Simulated mean yearly moisture flux partitioning of total precipitation at the different FLUXNET sites with JULES-orig (a) and with JULES-adapt (b).

Table 4
Ratio of transpiration (E_t), intercepted water evaporation (E_c) and soil evaporation (E_s) to evapotranspiration (ET) in JULES-orig and JULES-adapt for the entire period provided in Table 1.

	Bra	Bug	Cab	Gri	Hai	Hes	LeB	Loo	Tha	Vie	Wet	Mean
Orig.												
E_t/ET	0.27	0.38	0.48	0.64	0.51	0.51	0.34	0.25	0.38	0.48	0.45	0.42
E_c/ET	0.21	0.14	0.19	0.18	0.26	0.24	0.26	0.27	0.28	0.26	0.32	0.24
E_s/ET	0.52	0.48	0.32	0.18	0.22	0.24	0.42	0.47	0.35	0.26	0.24	0.34
Adapt.												
E_t/ET	0.47	0.69	0.59	0.79	0.64	0.75	0.63	0.53	0.60	0.62	0.78	0.65
E_c/ET	0.13	0.10	0.13	0.14	0.17	0.18	0.16	0.18	0.20	0.19	0.20	0.15
E_s/ET	0.39	0.21	0.28	0.07	0.19	0.08	0.22	0.30	0.19	0.19	0.02	0.20

forest and 0.6 for grassland. At the selected sites in this study, the transpiration accounts on average for only 42%, the soil evaporation for 34% and the intercepted water evaporation for 24% (see Table 4).

Very few measurements have been performed at site specific locations. Wilson et al. (2001) measured the contribution of transpiration, intercepted water and soil evaporation in temperate deciduous forests and found it to be 60%, 20% and 20%, respectively. A similar contribution of soil evaporation was observed for the temperate broad-leaved forest in Hainich (Bittner et al., 2010). During the summer however, the contribution of the soil dropped to 10–13%. At Brasschaat, the observed soil evaporation contributes about 30% to the total evapotranspiration (Meiresonne et al., 2003). At Vielsalm in 2011, the transpiration represented 53% and the intercepted water evaporation 13% (personal communication with R. Soubie and C. Vincke – 12/04/2013). Averaged over 14 stands in the North of Belgium, the contribution of transpiration is around 65%, that of intercepted water evaporation around 25% and of soil water evaporation 10% (Verstraeten et al., 2005). Sutanto et al. (2012) measured the evaporation fluxes during simulated summer conditions on a grassland. The fraction of transpiration, soil and intercepted water evaporation were 77.7%, 12.2% and 10.1%, respectively. Based on all these studies, the contribution of soil water evaporation in JULES is largely overestimated compared to the contribution of transpiration (see Table 4). The soil evaporation is particularly large at sites with sparse vegetation; i.e. Bug, Cab, Bra, LeB and Loo (see Table 1 for LAI values), where it represents between 32% and 52% of the total ET. The underestimation of the transpiration fraction is however less pronounced at the broad leaf forest sites (Hai and Hes).

In summary, JULES-orig captures the seasonal variability, but does not capture well spatial and inter-annual variability of the water and carbon fluxes. Compared to FLUXNET data, the GPP is underestimated and the evaporative flux overestimated. In addition to this, the latter flux is not well partitioned between its components; the transpiration is underestimated, and the soil evaporation is overestimated.

4.2. Impact of all combined adaptations to JULES v2.2

The simulations performed with the adapted model, *JULES adapt*, show an overall significant increase in gross assimilation (Fig. 2(a)) and a decrease in modelled evapotranspiration (Fig. 2(b)) compared to *JULES-orig*. The modelled mean yearly water and carbon fluxes present a smaller bias against the FLUXNET observations, with a strong reduction of the systematic over- and underestimation, respectively (see RMSE and MBE values in Table 3). The modelled mean yearly GPP now correlates well with the FLUXNET data (see *r* values in Table 3). This shows that the adaptations have improved the skill of the model in capturing the spatial variability. Concerning the temporal variability, the adaptations did not significantly improve the skill of the model in capturing the inter-annual variability (not shown). However, they improved the performance of the model at the monthly timescale (Fig. 5).

The lack of energy balance at the FLUXNET sites might partially explain the remaining discrepancy between observed and simulated evapotranspiration. Anthropogenic interferences can also play a role and explain the small inter-annual variability modelled at some sites. For example, at Gri the model strongly overestimated the actual GPP; the additional grass-cuts, in particular during 2004 and 2006 (Prescher et al., 2010), cannot be simulated with the model.

The significant decrease in simulated ET is mainly due to a decrease in soil evaporation, and to a lesser extent to a decrease in intercepted water evaporation (Fig. 4(d)). On average, at all sites, the evaporation rate, both of soil moisture and intercepted water, has decreased by 60%. At the sites with a large fraction of needle leaf trees (LeB, Loo, Tha and Wet) this reduction is partially compensated by an increase in transpiration rate. A strong increase in run-off is noticeable as well, except at the sites located on medium fine soils (Hes and Wet), where a slight reduction is simulated. The largest increase in run-off is simulated at sites located on sandy soils (Bra, Bug, LeB and Loo). The deep drainage rate has increased as well, except at needle leaf sites on sandy soils (LeB and Loo). Based on the values mentioned in Section 4.1 *JULES-adapt* shows a more realistic partitioning of the moisture flux (see Fig. 3(b) and Table 4). The transpiration rate represents now on average 65% of the total ET, the intercepted water evaporation 15% and the soil evaporation 20%. Overall the contribution of transpiration to the evaporative flux has increased by 50%, the contribution of the intercepted water evaporation has decreased by 30% and that of the soil evaporation by 50%.

The adaptations had also an impact on the extractable soil water content. The simulated extractable soil water content in the top soil layer, 0–0.1 m, increased significantly at all sites (Fig. 2(d)). In the sub-layer, 0.1–3 m depth, the content increased as well compared to the simulation performed with *JULES-orig*, except at Loo and LeB where the content decreased (Fig. 2(c)). Over the whole soil profile up to 3 m depth, the extractable soil water content remained unchanged at Loo and LeB. At those two sites the strong increase in run-off and transpiration was not counterbalanced enough by the decrease in soil and intercepted water evaporation. However, a strong reduction in drainage compensated for the increased water loss. The overall larger extractable soil moisture content, in particular during winter, enhanced the surface run-off.

An impact on the seasonal cycle of the soil moisture content was also noticeable. The soil moisture content simulated with JULES-adapt shows a lead-lag of two to four weeks with the content simulated with JULES-orig (see Figs. A.1 and A.2 in Appendix C). This lag is the largest at LeB and Bug; both sites are water stressed during summer. Next, compared to *JULES-orig*, the reduction in soil moisture content during spring and summer is weaker in JULES-adapt. This can be explained by the reduced evaporative flux, mainly during spring and early summer. At Loo, Tha and Wet, however, this reduction in ET is weak and constant during the entire year. A smaller evaporative flux during spring and summer and an

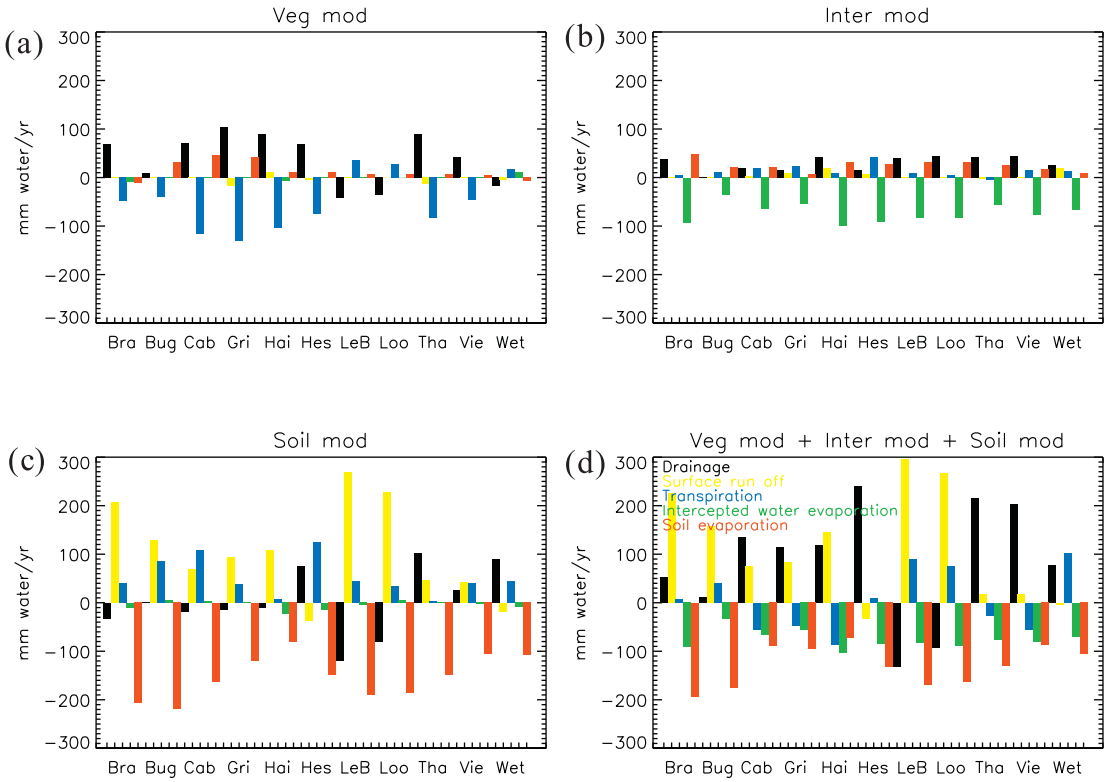

Fig. 4. Impact of the 'Veg mod' (a), 'Inter mod' (b), 'Soil mod' (c) adaptations and a combination of them (d) on the simulated mean yearly moisture flux partitioning at the different FLUXNET sites, in comparison with JULES-orig.

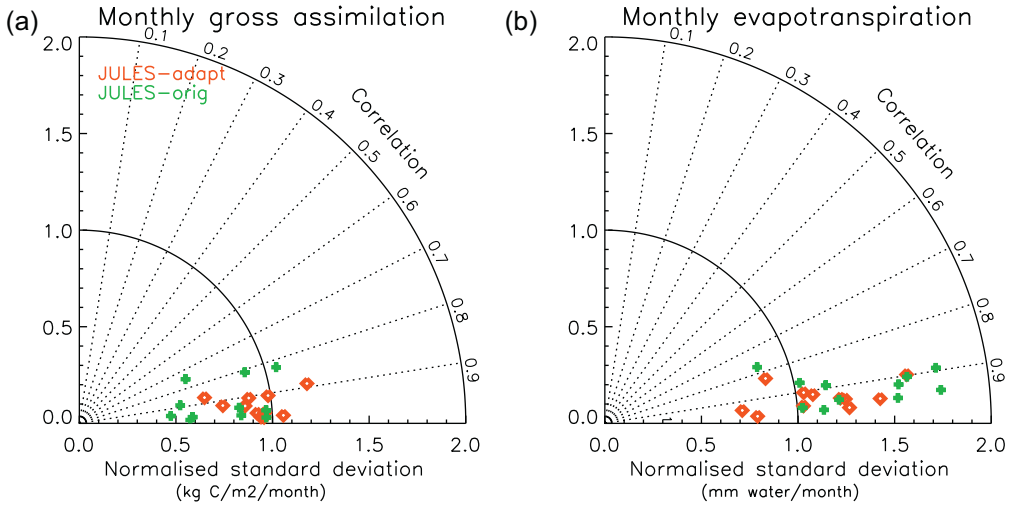

Fig. 5. Taylor diagram of the monthly GPP (a) and ET (b) at each site for the time series given in Table 1, with the JULES-orig simulations in green and the JULES-adapt in red. (For interpretation of the references to colour in this figure legend, the reader is referred to the web version of the article.)

overall larger soil moisture content lead to a smaller amplitude of the seasonal cycle of soil moisture.

Finally, as mentioned by Teuling et al. (2009), trends in ET are most likely induced by trends in the limiting driver. From Table 5 it can be seen that, compared to *JULES-orig* the modelling results have shifted from a soil moisture-limited regime to a more radiation-limited regime, except at Bug and LeB. The simulated evapotranspiration rate ET is now more positively correlated with the radiation than it is with the soil moisture content. These results correspond well to the observations made by Teuling et al. (2009), who found a clear North-South gradient in Europe, with a near-perfect linear correlation for

Table 5
Pearson correlation coefficient for the correlation between simulated ET and global radiation, and between ET and soil moisture content.

	Bug	Cab	Hai	Hes	LeB	Loo	Tha	Vie	Wet
ET versus radiation									
Orig	0.16	−0.59	0.74	−0.28	−0.13	0.05	0.57	0.9	−0.46
Adapt.	0.09	−0.36	0.87	0.35	−0.4	0.22	0.78	0.97	0.90
ET versus soil moisture									
Orig	0.96	0.77	−0.53	0.76	0.76	0.43	0.67	0.011	0.27
Adapt.	0.96	0.31	−0.52	−0.58	0.81	0.015	0.23	−0.31	−0.74

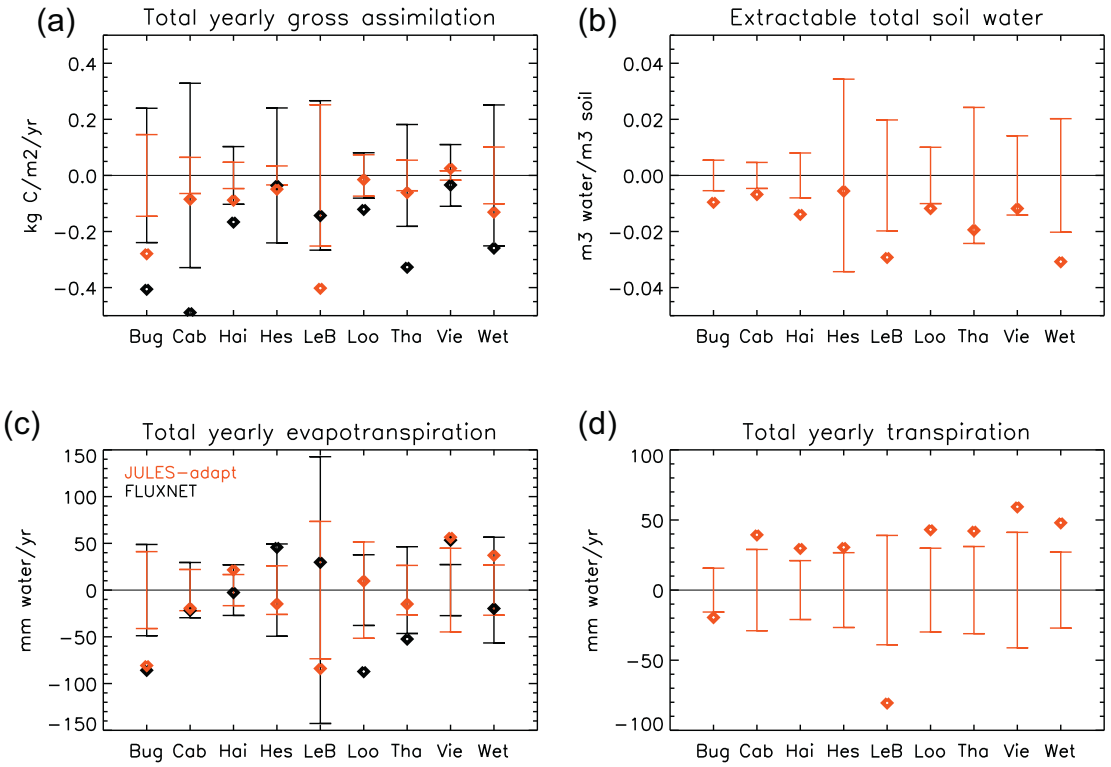

Fig. 6. The 2003 anomalies and the one standard deviation of the inter-annual variability of the mean yearly GPP (a), extractable soil water over 3 m depth (b), evapotranspiration (c) and transpiration (d), with the FLUXNET data in black and the JULES-adapt simulations in red. (For interpretation of the references to colour in this figure legend, the reader is referred to the web version of the article.)

radiation in Central Europe and Scandinavia, decreasing towards the Mediterranean.

4.2.1. Role of the individual adaptations applied to JULES v2.2

The reduced bias and the improved correlation between the simulated and observed GPP are mainly due to the adaptations made to the vegetation physiology *Veg-mod* (see Table 3). The *Veg-mod* adaptations also improved the correlation between observed and simulated evaporative flux. However, the reduction in bias of this flux was mainly due to the adaptations made to the soil evaporation and infiltration *Soil-mod* and to the intercepted water evaporation *Inter-mod* (see Table 3).

The adaptations made to the vegetation physiology, *Veg-mod*, significantly increased the GPP at the grassland sites and at the sites with an important fraction of needle leaf trees, and reduced the evaporative flux at sites with an important fraction of broad leaf trees, through a reduction in their transpiration rate (Fig. 4(a)). As mentioned in Section 3.1.1, the net photosynthesis A is limited by low values of C_i (Collatz et al., 1991, 1992), which is positively correlated with f_0. From Eq. (2) it follows that the $C_c - C_i$ gradient is increased for low values of f_0. Both effects result in a reduction of the stomatal conductance and transpiration when f_0 decreases, which is the case for the *Veg-mod* set-up compared to JULES-orig. At the needle leaf sites, this reduction in transpiration rate is however compensated by an increase in carboxylation rate, through an increase in n_l value. This increase in carboxylation rate enhances the photosynthetic rate, which explains the increase in gross assimilation at the needle leaf sites, and consequently, the stomatal conductance (Eq. (1)). This means that the reduction in f_0 only affected the transpiration and, to a lesser extent, the photosynthetic rate of the broad leaf trees and C3 grasses. The reduction in transpiration rate at those sites however resulted in a water saving. This limited the water stress experienced by vegetation at some sites during spring and summer and, by consequence, slightly enhanced the GPP. In addition, it increased the drainage rate. Finally, the decrease in transpiration was slightly compensated by an increase in soil evaporation to fulfil the evaporative demand of the atmosphere.

The adaptations made to the soil evaporation and infiltration, *Soil-mod*, are responsible for the strong decrease in soil evaporation and increase in run-off, except at Hes and Wet, where the run-off rate has decreased compared to *JULES-orig* (Fig. 4(c)). By converting the medium fine top soil layer texture of those two sites into an organic layer, the saturated hydraulic conductivity K_s of this top soil layer was increased threefold (see Table A.2). At all the other sites K_s has been decreased, with a very strong decrease for the *coarse* texture soil. This explains the strong reduction in infiltration rate and increase in run-off at Bra, Bug, LeB and Loo. This means that the impact of *Soil-mod* on the moisture flux components depends strongly on the soil texture; the sensitivity is larger for a land surface on sandy soils. *Soil-mod* is also responsible for the increase in extractable water content in the top soil layer. The increase in this layer is mainly due to the change in soil texture, and by consequence in maximum extractable soil moisture (see Table A.2). Overall the reduction in soil evaporation is partially compensated by an increase in transpiration to fulfil the evaporative demand of the atmosphere.

The adaptations made to the intercepted water evaporation, *Inter-mod*, are responsible for a decrease in intercepted water evaporation (Fig. 4(b)). The contribution of this component to the total evapotranspiration rate has decreased by more than half at Bra, Bug, Cab, Hai, Hes, LeB and Vie. These sites are the two broad leaf tree sites; i.e. Hai and Hes, the mixed forest sites with a large fraction of broad leaf trees; i.e. Vie, and the sites with sparse vegetation coverage; i.e. Bra, Bug, Cab and LeB. For more information on the vegetation coverage, we refer to Table 1. The reduction in intercepted water evaporation at the broad leaf and mixed forest sites takes place mainly during winter, when the canopy is leafless, and

during the entire year for sites with sparse coverage. This is due to the fact that a lower interception capacity has now been assigned to soil and leafless trees (see Eqs. 9 and 10). With our adaptations, its dependency on LAI has been enhanced. The sensitivity of the model to the *'Inter-mod'* adaptations depends strongly on the land surface coverage; the impact on the moisture flux partitioning is more important for a land surface covered by broadleaf trees, due to its seasonality and for a land surface with sparse vegetation coverage. The decrease in intercepted water evaporation is partially compensated by an increase in soil evaporation and, to a lesser extent, by an increase in transpiration (Fig. 4(b)). In addition to this, as the amount of intercepted water is reduced, there is a slight increase in throughfall and infiltration and, by consequence, a slightly larger amount of water in the sub-soil layers. This explains the higher drainage rate.

4.3. The extreme event of 2003 as benchmark

The results of the simulation performed with *JULES-adapt* have been evaluated for the extreme event of 2003. Bra and Gri are not included in this analysis, as no data were available for this year.

From Fig. 6(a) it can be seen that the anomalies of the simulated GPP for 2003 are all negative, except at Vie, and located at the lower end of one standard deviation of the inter-annual variability. This is similar to the fingerprint shown by the FLUXNET data. The anomalies simulated with JULES-adapt are however underestimated compared to the observed values. During 2003 the simulated GPP was on average reduced by 10% only, compared to the mean values over the time series provided in Table 1. At the FLUXNET sites a reduction of 30% has been observed in 2003 compared to 2002 (Ciais et al., 2005). This difference between simulations and observations might be due to the fact that in the model the phenology is prescribed and that it does not simulate early leaf yellowing and litter fall due to drought (Le Dantec et al., 2000). These processes would decrease the GPP. At Hesse, for example, important leaf fall in mid-August was observed (Granier et al., 2007). In addition to this, Zaitchik et al. (2006) demonstrated that the early vegetation green-up due to the springtime warmth, together with the lack of precipitation, resulted in an early season soil moisture deficit. This cannot be simulated by the setup chosen for our modelling system, because of the prescribed phenology.

Fig. 6(b) indicates that there is a good correlation between the GPP and the soil moisture anomalies during the 2003 extreme event. Similar to the observations made by Reichstein et al. (2002), there is a positive response of the simulated GPP to the simulated soil moisture content during the July-September period (not shown). The non-significant negative GPP anomalies observed at Vie in 2003 (Fig. 6(a)) could be due to the fact that in 2003 this site experienced a moderate drought intensity that did not reduce the stomatal conductance to a large extent and for a limited period only, while the generally higher radiation that was observed in summer 2003 resulted in enhanced photosynthesis (Granier et al., 2007).

Besides the good correlation with the soil moisture depletion, the drop in modelled GPP during 2003 seems to coincide with a reduced ET, except at 3 sites (Hai, Loo and Wet) (Fig. 6). The reduction in ET is very strong (larger than one standard deviation of the inter-annual variability) at two sites; i.e. Bug and LeB. At those two sites the decrease in ET is due to a decrease of both transpiration and evaporation rates. At the remaining sites, the simulated transpiration rate has increased in 2003. The decrease in ET at those sites is therefore due to a strong decrease in evaporation. Although the stomatal conductance was limited due to water stress, the evapotranspiration was not reduced to a large extent. The stronger positive radiation anomaly in 2003 (Fischer and Seneviratne, 2007) enhanced the evaporative demand. In combination with low precipitation rate, it enhanced the depletion of the intercepted water

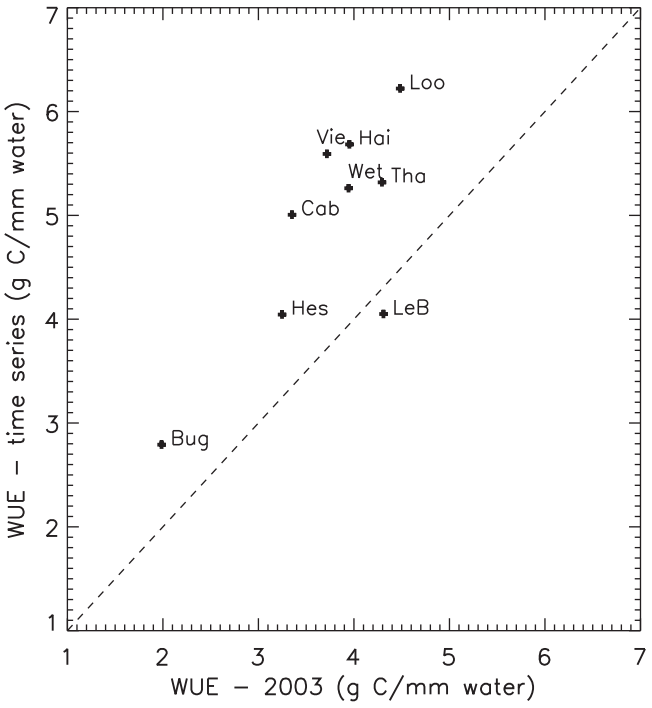

Fig. 7. Correlation between the yearly mean WUE simulated with JULES-adapt at the different sites in 2003 and the mean value over the whole time series during the July–September period.

reservoir (fast reservoir) followed by the depletion of the top soil water reservoir (intermediate reservoir). A higher water extraction through transpiration from the deeper soil layers (slow reservoir) tended to compensate for a reduced evaporation from the depleted fast and intermediate reservoirs. This was simulated at Hes, Loo and Tha (Figs. A.1 and A.2). Once the deeper soil layers started to deplete, the transpiration rate decreased as well. This was the case at Bug and LeB. These results show that the good correlation between the carbon flux and the water flux anomalies is not only due to the effect of water stress on vegetation (through stomatal conductance) as mentioned by Reichstein et al. (2002) and Granier et al. (2007); depletion of the fast and intermediate reservoir plays an important role as well.

Fig. 7 shows the correlation between the simulated mean water use efficiency, WUE, which is computed as the ratio between the cumulated GPP and transpiration for the period July–September over the entire time-series, and the simulated WUE during 2003 for the same period. At almost all sites the WUE during the drier 2003 is lower than for an average year (climatology), except at LeB. This pattern of lower WUE efficiency under dry conditions corresponds well with the observations made by Reichstein et al. (2007). The increase in WUE with soil moisture content is due to a larger sensitivity of GPP rather than of transpiration to soil moisture content, except at LeB. Similar findings were reported by Kuglitsch et al. (2008).

5. Conclusions

In this study, the land surface model JULES has been evaluated against 11 European temperate FLUXNET sites: 8 forests sites and 3 grassland sites. The results show that the original model formulation (Essery et al., 2001; Clark et al., 2011; Best et al., 2011) captures the seasonal variability, but does not credibly represent the spatial and inter-annual variability of the water and carbon fluxes. The inability of representing the inter-annual variability is still a major problem for the majority of land surface models (Keenan et al.,

2012). Compared to FLUXNET data, the GPP simulated with JULES is underestimated and the evaporative flux overestimated. Additionally, most published studies for the temperate regions indicate that, on an annual basis, transpiration is the dominant component on the land surface, followed by soil and intercepted water evaporation. The original JULES formulation, however, does not reflect this ET partitioning, with soil and intercepted water evaporation far outweighing transpiration.

In this study a range of adaptations are suggested to alleviate these long-standing biases: these consist of changes in parameterisation and process representations for vegetation transpiration, intercepted water evaporation and soil water availability, evaporation and infiltration. The individual adaptations have been clearly shown to be beneficial in alleviating specific biases in the model. The combined adaptations have improved the performance of the model in simulating the spatial and temporal variability of the carbon and water fluxes. In addition, they increased the accuracy of the simulated GPP and ET. The most significant improvement is the overall decrease in evaporative flux by 30%.

The adapted model exhibits significant improvements in its partitioning of evapotranspiration; transpiration is now the largest component. The reduction of the depth of the top soil layer available for soil evaporation prevents excessive loss of soil moisture to evaporation. The reduced capacity and evaporation from the interception reservoir increases the amount of water that can reach the ground and infiltrate into the soil. Overall the adaptations resulted in wetter soils, and by consequence in larger drainage rates. An increase in surface run-off is a consequence of the higher soil moisture content noticed at some sites and the reduced infiltration enhancement factor. These changes in partitioning have a large impact on the overall surface water balance, and by consequence are expected to feedback on the atmosphere once JULES-adapted is coupled back to the Met Office GCM.

Since the transpiration component, compared to the evaporation components, is more important in the adapted version, one would anticipate the ET response to a rain event in the adapted version to be slightly delayed and to extend for a longer time period. A soil moisture lag correlation of two weeks to one month between JULES-orig and JULES-adapt was indeed simulated, with a larger lag at moisture stressed sites. This is indicative of a longer climate memory, modulated by soil water, which is relevant to the problem of land–atmosphere coupling and is expected to improve the standing of the UK's Unified Model system in GCM intercomparisons (Koster et al., 2006). Moreover, compared to JULES-orig, the simulated ET has shifted from a soil moisture limited regime to a more radiation limited regime. As trends in radiation (global dimming and brightening) are expected to impact ET only in regions where ET correlates with radiation (Teuling 2009), these adaptations are expected to affect climate simulations over Europe.

Next, the results of the simulation performed for the extreme event of 2003 were used as evaluation benchmark for the adapted version of the model to simulate climate change scenarios. JULES-adapt captures the impact of the 2003 drought on the carbon assimilation and WUE. However the model underestimates the 2003 anomalies overall. This might be due to the fact that the model phenology is prescribed, so that JULES is unable to interactively simulate early vegetation green-up, early leaf yellowing and litter fall. An appropriate description of groundwater dynamics is also crucial for evaluating drought stress; varying soil depth, rooting depth and dynamics, groundwater table and capillary rise are not represented in JULES. An interactive phenology as well as an improved representation of the response of plants to water stress will very likely enhance the sensitivity of the vegetation to extreme events.

The results of the 2003 simulations also showed that the good correlation between the carbon and the water fluxes anomalies is not solely due to the effect of water stress on vegetation (through stomatal conductance) as mentioned by Reichstein et al. (2002) and Granier et al. (2007): depletion of the fast and intermediate reservoirs plays an important role as well. This highlights the importance of process studies at the components level: for instance, confronting the model with a single evapotranspiration field from observations is an insufficient test of model fidelity. More detailed and complex measurements of moisture flux partitioning are needed to better evaluate the models used in weather and climate prediction.

Finally, this study suggests that the impact of the soil structure and texture on the moisture flux and its partitioning is as important as vegetation structure and composition. Both soil and vegetation are in fact strongly linked in nature; soil type affects vegetation type, and vice versa.

In the near future, we intend to investigate the impact of our adaptations in the context of coupled land–atmosphere simulations, and in particular the effect of the adaptations on the diurnal cycle of fluxes and Bowen ratio (=SH/LE). We have already shown in this study that more of the available surface energy is devoted to sensible heat rather than latent heat flux (larger Bowen ratio). If coupled to a GCM, the resulting planetary boundary layer will be relatively deeper. The reduced moisture flux into a deep boundary layer leads to an anomalously dry and therefore more stable boundary layer (Eltahir, 1998), but it may also alter the moisture conversion over land (Schär et al., 1999). As the Bowen ratio of the land surface modulates the thermodynamics and the dynamics of atmospheric circulation, these adaptations might affect the surface-climate feedback (Lawrence et al., 2006).

Acknowledgments

The authors would like to thank the PIs of the eleven European Eddy Fluxes Database sites for providing the required data for this study. C. Van den Hoof was funded by the SWELTER-21 project (Soil Water – Climate Feedbacks in Europe in the 21st Century (NERC: NE/I006834/1)).

Appendix A. Accronyms

See Table A.1.

Appendix B. Hydraulic parameters

See Table A.2.

Appendix C. Seasonal cycle

See Figs. A.1 and A.2.

Tabel A.1
Definition of acronyms.

Symbol	Units	Definition
a	–	parameter of the simplified formulation developed by Leuning (1995)
A	mol CO_2 m^2 s^{-1}	net leaf photosynthesis rate
α	m^{-1}	van Genuchten fitting parameter
BL	–	broad-leaf trees
β	–	infiltration enhancement factor
C	kg m^{-2}	canopy moisture content
C_c	Pa	leaf surface CO_2 partial pressure
C_i	Pa	internal CO_2 partial pressure
C_m	kg m^{-2}	canopy capacity
C3	–	plant that utilises the C_3 carbon fixation pathway
C4	–	plant that utilises the C_3 carbon fixation pathway
d	m	displacement height
D_c	kg H_2O kg^{-1} air	critical humidity deficit
D_*	kg H_2O kg^{-1} air	humidity deficit at the leaf surface
ET	mm $time^{-1}$	evapotranspiration
E_c	mm $time^{-1}$	intercepted water evaporation
E_s	mm $time^{-1}$	soil evaporation
E_t	mm $time^{-1}$	transpiration
f_0	–	maximum ratio between intercellular and atmospheric CO_2
f_a	–	saturated fraction of the canopy
GPP	kg CO_2 $time^{-1}$	gross primary productivity
g_s	m s^{-1}	stomatal conductance
g_{soil}	m s^{-1}	soil conductance
Γ	Pa	photorespiration compensation point
h	m	height of vegetation
H	m	height of eddy flux measurements
K_s	mm s^{-1}	soil saturated hydraulic conductivity
K	mm s^{-1}	surface infiltration rate
m		shape parameter of the water retention curve
LAI	m^2 m^{-2}	leaf area index
LE	W m^2	latent heat
n	–	shape parameter of the water retention curve
n_l	kg N kg^{-1} C	leaf nitrogen concentration
NEE	kg CO_2 $time^{-1}$	net ecosystem exchange
NL	–	needle-leaf trees
p	Pa	surface pressure
P	mm $time^{-1}$	precipitation
PFT	–	plant functional type
ψ	Pa	pressure head
q	kg kg^{-1}	air humidity
R	J K^{-1} mol^{-1}	prefect gas constant
R_g	W m^{-2}	global radiation
R_n	W m^{-2}	net radiation
SH	W m^{-2}	sensible heat
S_n	mm $time^{-1}$	snow
T	K or °C	air temperature
T_*	K	leaf surface temperature
θ_c	m^3 m^{-3}	volumetric soil moisture content at critical point
θ_r	m^3 m^{-3}	residual water content
θ_{sat}	m^3 m^{-3}	volumetric soil moisture content at saturation
θ_w	m^3 m^{-3}	volumetric soil moisture content at wilting point
θ_1	m^3 m^{-3}	volumetric soil moisture content in the top 0.1 m of the soil
V_m	mol CO_2 m^2 s^{-1}	maximum rate of carboxylation of Rubisco
V_{max}	mol CO_2 m^2 s^{-1}	maximum rate of carboxylation of Rubisco at 25 °C
$\|v\|$	m s^{-1}	wind speed
WUE	kg CO_2 m^{-2} mm^{-1} H_2O	water use efficiency

Tabel A.2
Wösten parameters for JULES: the volumetric water content at saturation (θ_s), at the critical point (θ_c) and at the wilting point (θ_w), the saturated hydraulic conductivity (K_s), the fitting parameters α and the shape parameter of the water retention curve n.

	θ_r (m^3 m^{-3})	θ_s (m^3 m^{-3})	θ_c (m^3 m^{-3})	θ_w (m^3 m^{-3})	K_s (mm s^{-1})	$1/\alpha$	$1/(n-1)$ (=m)
Topsoil							
Coarse	0.025	0.40	0.17	0.059	0.00694	0.261	2.65
Medium	0.010	0.44	0.29	0.15	0.00140	0.318	5.54
Medium fine	0.010	0.43	0.32	0.13	0.00026	1.205	9.94
Fine	0.010	0.52	0.40	0.28	0.00288	0.272	9.88
Very fine	0.010	0.61	0.49	0.33	0.00174	0.377	9.68
Subsoils							
Coarse	0.025	0.37	0.11	0.04	0.00810	0.233	1.92
Medium	0.010	0.39	0.27	0.15	0.00124	0.402	5.92
Medium fine	0.010	0.41	0.32	0.15	0.00046	1.22	4.59
Fine	0.010	0.48	0.41	0.3	0.00098	0.505	11.6
Very fine	0.010	0.54	0.47	0.36	0.00095	0.595	13.7
Organic	0.010	0.77	0.56	0.27	0.00093	0.769	4.9

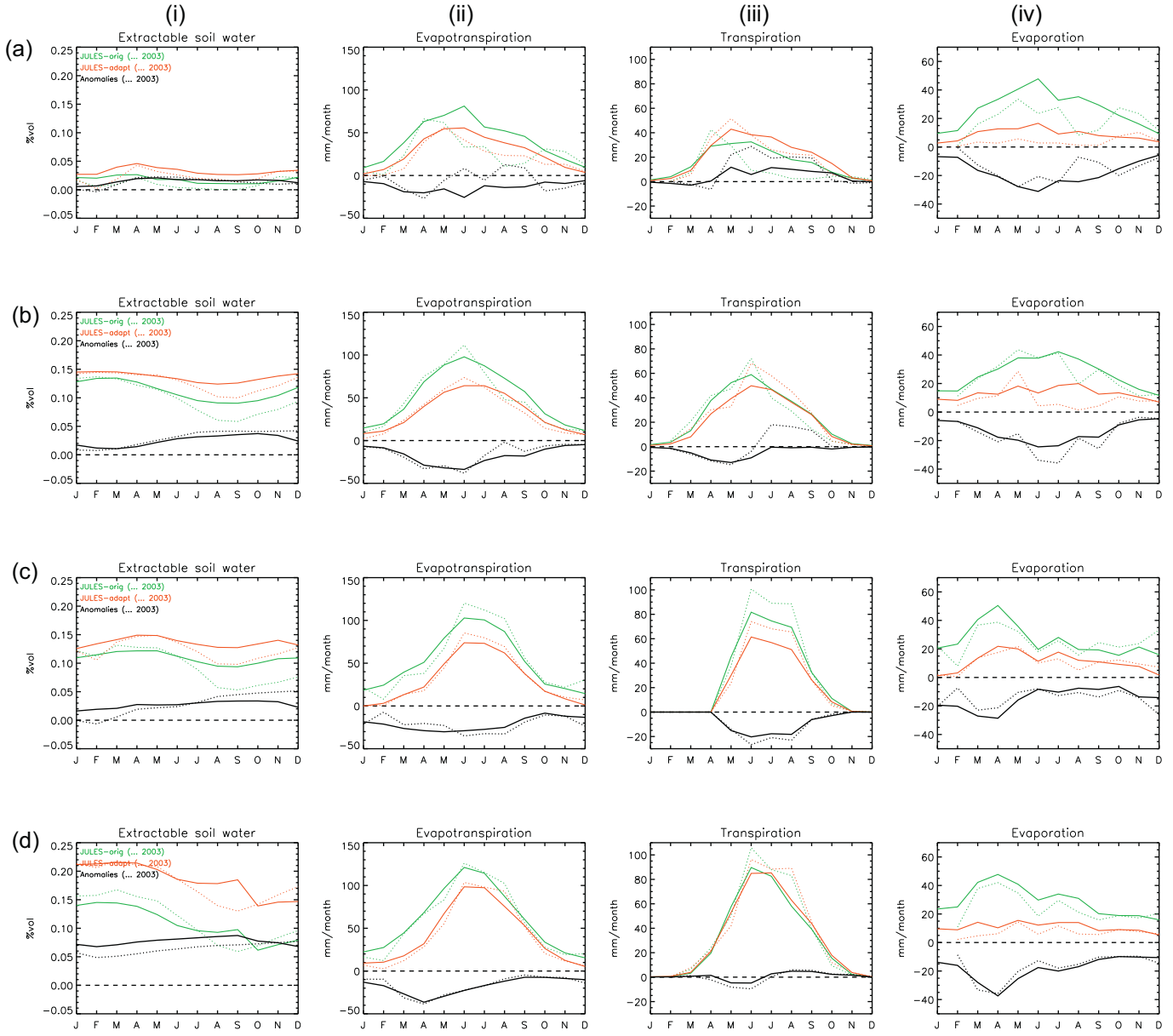

Fig. A.1. The seasonal cycle of the volumetric extractable soil moisture within 3 m depth (i), ET (ii), E_t (iii) and $E_s + E_c$ (iv) simulated over the entire time series with JULES-orig in green and with JULES-adapt in red, with the values for 2003 as dotted lines for Bug (a), Cab (b), Hai (c) and Hes (d). The anomalies between JULES-adapt and JULES-orig are in plain black lines for the entire time series and by dotted black lines for 2003. (For interpretation of the references to colour in this figure legend, the reader is referred to the web version of the article.)

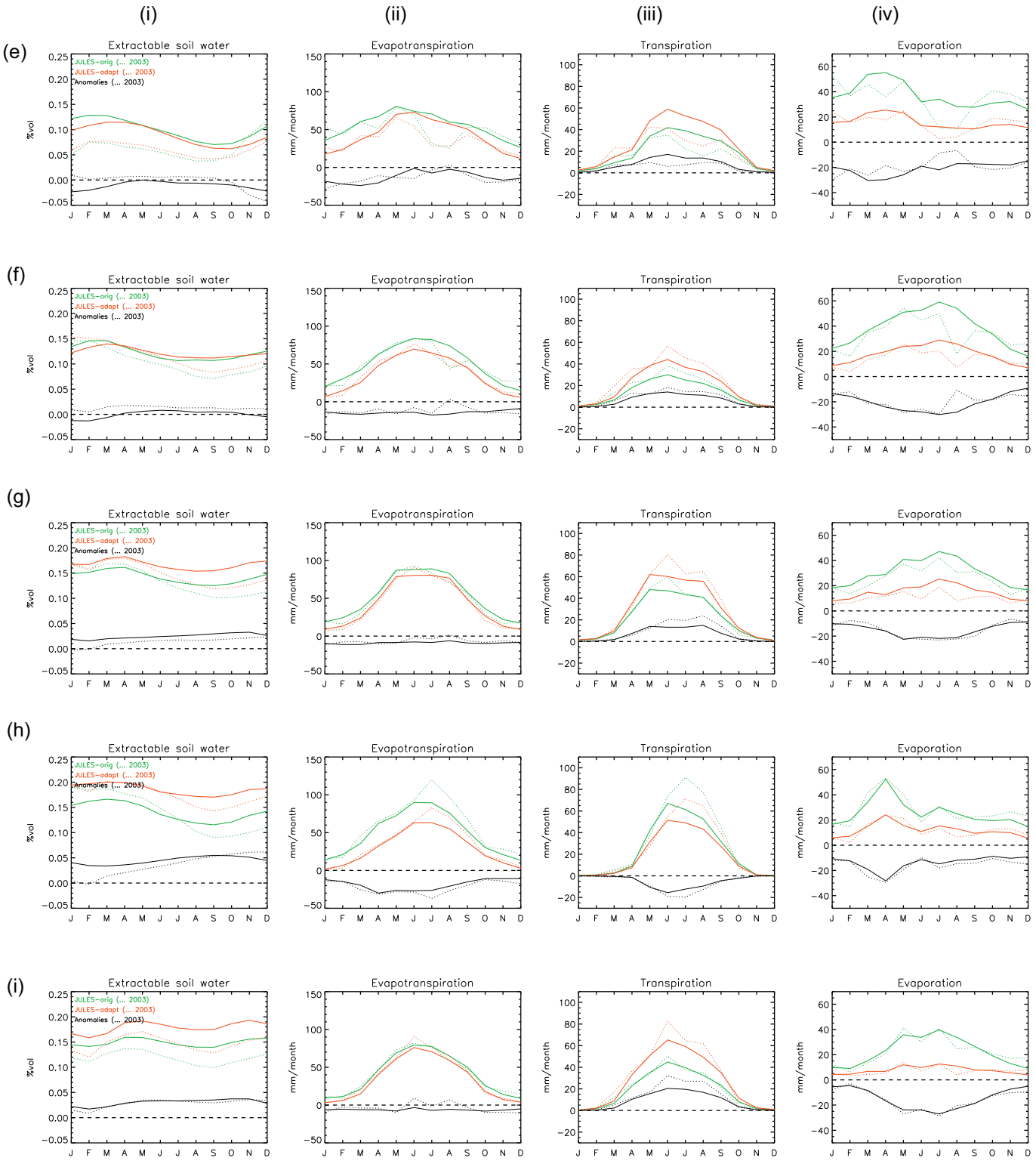

Fig. A.2. These plots represent the same variables as Fig. A.1, but for LeB (e), Loo (f), Tha (g), Vie (h) and Wet (i).

References

Anthoni, P., Knohl, A., Rebmann, C., Freibauer, A., Mund, M., Ziegler, W., Kolle, O., Schulze, E.-D., 2004. Forest and agricultural land-use-dependent CO_2 exchange in Thuringia, Germany. Global Change Biol. 10, 2005–2019.

Aubinet, M., Chermanne, B., Vandenhaute, M., Longdoz, B., Yernaux, M., Laitat, E., 2001. Long term carbon dioxide exchange above a mixed forest in the Belgian Ardennes. Agric. For. Meteorol. 108, 293–315.

Aubinet, M., Grelle, A., Ibrom, A., Rannik, U., Moncrieff, J., Foken, T., Kowalski, A., Martin, P., Martin, P., Berbigier, P., Bernhoffer, C., Clement, R., Elbers, J., Granier, A., Grunwald, T., Morgenstern, K., Pilegaard, K., Rebmann, C., Snijders, S., Valentini, R., Vesala, T., 2000. Estimates of the annual net carbon and water exchange of forests: the EUROFLUX methodology. Global Change Biol. 30, 113–175.

Aubinet, M., Heinesch, B., Longdoz, B., 2002. Estimation of the carbon sequestration by a heterogeneous forest: night flux corrections, heterogeneity of the site and inter-annual variability. Global Change Biol. 8, 1053–1071.

Baldocchi, D., Ryu, Y., 2011. A Synthesis of Forest Evaporation Fluxes – from Days to Years – as Measured with Eddy Covariance. No. 216. Springer Science, Ch. Forest Hydrology and Biogeochemistry: Synthesis of Past Research and Future Directions, Ecological Studies., pp. 101–116.

Balogh, J., Pintér, K., Fóti, S., Cserhalmi, D., Papp, M., Nagy, Z., 2011. Dependence of soil respiration on soil moisture, clay content, soil organic matter, and CO_2 uptake in dry grasslands. Soil Biol. Biochem. 43, 1006–1013.
Berbigier, P., Bonnefond, J.-M., Mellmann, P., 2001. CO_2 and water vapour fluxes for 2 years above Euroflux forest site. Agric. For. Meteorol. 108, 183–197.
Best, M., Pryor, M., Clark, D., Rooney, G., Essery, R., Ménard, C., Edwards, J., Hendry, M., Porson, A., Gedney, N., Mercado, L., Sitch, S., Blyth, E., Boucher, O., Cox, P., Grimmond, C., Harding, R., 2011. The Joint UK Land Environment Simulator (JULES), Model description – Part 1: Energy and water fluxes. Geosci. Model Dev. Discuss. 4, 595–640.
Betsch, P., Bonal, D., Breda, N., Montpied, P., Peiffer, M., Tuzet, A., Granier, A., 2011. Drought effects on water relations in beech: the contribution of exchangeable water reservoirs. Agric. For. Meteorol. 151, 531–543.
Betts, R.A., 2007. Implications of land ecosystem–atmosphere interactions for strategies for climate change adaptation and mitigation. Tellus B 59, 602–615.
Bittner, S., Talkner, U., Krämer, I., Beese, F., Hölscher, D., Priesack, E., 2010. Modeling stand water budgets of mixed temperate broad-leaved forest stands by considering variations in species specific drought response. Agric. For. Meteorol. 150, 1347–1357.
Blyth, E., Gash, J., Lloyd, A., Pryor, M., Weedon, G., Shuttleworth, J., 2010. Evaluating the JULES land surface model energy fluxes using fluxnet data. J. Hydrometeorol. 11, 509–519.
Boone, A., Habets, F., Noilhan, J., Clark, D., Dirmeyer, P., Fox, S., Gusev, Y., Haddeland, I., Koster, R., Lohmann, D., Mahanama, S., Mitchell, K., Nasonova, O., Niu, G.-Y., Pitman, A., Polcher, J., Shmakin, A., Tanaka, K., van den Hurk, B., Vérant, S., Verseghy, D., Viterbo, P., Yang, Z.-L., 2004. The Rhône-aggregation land surface scheme intercomparison project: an overview. J. Clim. 17, 187–208.
Breuer, L., Eckhardt, K., Frede, H., 2003. Plant parameter values for models in temperate climates. Ecol. Model. 169, 237–293.
Brutsaert, W., 1982. Evaporation into the Atmosphere: Theory, History, and Applications. Kluwer Academic, Dordrecht, The Netherlands.
Carrara, A., Kowalski, A.S., Neirynck, J., Janssens, I.A., Yuste, J.C., Ceulemans, R., 2003. Net ecosystem CO_2 exchange of mixed forest in Belgium over 5 years. Agric. For. Meteorol. 119, 209–227.
Choudhury, B., DiGirolamo, N., 1998. A biophysical process-based estimate of global land surface evaporation using satellite and ancillary data – I. Model description and comparison with observations. J. Hydrol. 205, 164–185.
Ciais, P., Reichstein, M., Viovy, N., Granier, A., Ogée, J., Allard, V., Aubinet, M., Buchmann, N., Bernhofer, C., Carrara, A., Chevallier, F., de Noblet, N., Friend, A., Friedlingstein, P., Grünwald, T., Heinesch, B., Keronen, P., Knohl, A., Krinner, G., Loustau, D., Manca, G., Matteucci, G., Miglietta, F., Ourcival, J., Papale, D., Pilegaard, K., Rambal, S., Seufert, G., Soussana, J., Sanz, M., Schulze, E., Vesala, T., Valentini, R., 2005. Europe-wide reduction in primary productivity caused by the heat and drought in 2003. Nature 437, 529–533.
Clapp, R., Hornberger, G., 1978. Empirical equations for empirical equations for some soil hydraulic properties. Water Resour. Res. 14, 601–604.
Clark, D., Mercado, L., Sitch, S., Jones, C., Gedney, N., Best, M., Pryor, M., Rooney, G., Essery, R., Blyth, E., Boucher, O., Harding, R., Huntingford, C., Cox, P., 2011. The Joint UK Land Environment Simulator (JULES), model description – Part 2: Carbon fluxes and vegetation dynamics. Geosci. Model Dev. 4, 701–722.
Clausnitzer, F., Köstner, B., Schwärzel, K., Bernhofer, C., 2011. Relationships between canopy transpiration, atmospheric conditions and soil water availability – analyses of long-term sap-flow measurements in an old Norway spruce forest at the Ore Mountains/Germany. Agric. For. Meteorol. 151, 1023–1034.
Collatz, G.J., Ball, J.T., Grivet, C., Berry, J.A., 1991. Physiological and environmental regulation of stomatal conductance, photosynthesis and transpiration: a model that includes a laminar boundary layer. Agric. For. Meteorol. 54, 107–136.
Collatz, G.J., Ribas-Carbo, M., Berry, J.A., 1992. Coupled photosynthesis-stomatal conductance model for leaves of C_4 plants. Aust. J. Plant Physiol. 19, 519–538.
Cox, P.M., Betts, R., Bunton, C., Essery, R., Rowntree, P., Smith, J., 1999. The impact of new land surface physics on the GCM simulation of climate and climate sensitivity. Clim. Dyn. 15, 183–203.
Cox, P.M., Huntingford, C., Harding, R.J., 1998. A canopy conductance and photosynthesis model for use in a GCM land surface scheme. J. Hydrol. 212, 79–94.
Curiel Yuste, J., Konôpka, B., Janssens, I.A., Coenen, K., Xiao, C.W., Ceulemans, R., 2005. Contrasting net primary productivity and carbon distribution between neighboring stands of *Quercusrobur* and *Pinussylvestris*. Tree Physiol. 25, 701–712.
Deardorff, J., 1978. Efficient prediction of ground surface temperature and moisture, with inclusion of a layer of vegetation. J. Geophys. Res. 83C, 1889–1903.
Dickinson, R., Henderson-Sellers, A., Kennedy, P., 1993. Biosphere–Atmosphere Transfer Scheme (BATS) version 1e as coupled to the NCAR Community Climate Model, Tech. rep. National Center for Atmospheric Research.
Dirmeyer, P., 2011. A history and review of the global soil wetness project (GSWP). J. Hydrometeorol. 12, 729–749.
Dolman, A., Moors, E., Elbers, J., 2002. The carbon uptake of a mid latitude pine forest growing on sandy soil. Agric. For. Meteorol. 111, 157–170.
Eltahir, E., 1998. A soil moisture–rainfall feedback mechanism – 1. Theory and observations. Water Resour. Res. 34, 765–776.
Essery, R., Best, M., Cox, P., 2001. MOSES 2.2 technical documentation. Tech. rep. Hadley Centre.
Falge, E., Tenhunen, J., Baldocchi, D., Aubinet, M., Bakwind, P., Berbigier, P., Bernhofer, C., Bonnefond, J.-M., Burba, G., Clement, R., Davis, K., Elbers, J., Falk, M., Goldstein, A., Grelle, A., Granier, A., Grünwald, T., Gu?mundsson, J., Hollinger, D., Janssens, I.A., Keronen, P., Kowalski, A., Katul, G., Law, B., Malhi, Y., Meyers, T., Monson, R., Moors, E., Munger, J., Oechel, W., Tha Paw, U.K., Pilegaard, K., Rannik, U., Rebmann, C., Suyker, A., Thorgeirsson, H., A. Turnipsee, G.T., Wilson, K., Wofsy, S., 2002. Phase and amplitude of ecosystem carbon release and uptake potentials as derived from FLUXNET measurements. Agric. For. Meteorol. 113, 75–95.
Fischer, E., Seneviratne, S., 2007. Soil moisture–atmosphere interactions during the 2003 European summer heat wave. J. Clim. 20, 5081–5099.
Fischer, E., Seneviratne, S., Lüthi, D., Schär, C., 2007. Contribution of land–atmosphere coupling to recent European summer heat waves. Geophys. Res. Lett. 34, 1–6.
Flechard, C., Nemitz, E., Smith, R., Fowler, D., Vermeulen, A., Bleeker, A., Erisman, J., Simpson, D., Zhang, L., Tang, Y., Sutton, M., 2011. Dry deposition of reactive nitrogen to European ecosystems: a comparison of inferential models across the NitroEurope network. Atmos. Chem. Phys. 11, 2703–2728.
Foken, T., Aubinet, M., Finnigan, J., Leclerc, M., Mauder, M., Tha Paw, U.K., 2011. Results of a panel discussion about the energy balance closure correction for trace gases. Bull. Am. Meteorol. Soc. 92 (4), 13–18.
Foley, J., DeFrie, R., Asner, G., Barford, C., Bonan, G., Carpenter, S., Chapin, S., Coe, M., Daily, G., Gibbs, H., Helkowski, J., Holloway, T., Howard, E., Kucharik, C., Monfreda, C., Patz, J., Prentice, I., Ramankutty, N., Snyder, P., 2005. Global consequences of land use. Science 309 (5734), 570–574.
Gedney, N., Cox, P., Douville, H., Polcher, J., Valdes, P., 2000. Characyerizing GCM land surface schemes to understand their response to climate change. J. Clim. 13, 3066–3079.
Gibelin, A.-L., Calvet, J.-C., Roujean, J.-L., Jarlan, L., Los, S., 2006. Ability of the land surface model ISBA-A-gs to simulate leaf area index at the global scale: comparison with satellites products. J. Geophys. Res. 111, 1–16.
Gibelin, A.-L., Calvet, J.-C., Viovy, N., 2008. Modelling energy and CO_2 fluxes with an interactive vegetation land surface model-evaluation at high and middle latitudes. Agric. For. Meteorol. 148, 1611–1628.
Gielen, B., Verbeeck, H., Neirynck, J., Sampson, D., Vermeiren, F., Janssens, I., 2010. Decadal water balance of a temperate Scots pine forest (*Pinussylvestris* L.) based on measurements and modelling. Biogeosciences 7, 1247–1261.
Gilmanov, T., Soussana, J., Aires, L., Allard, V., Ammann, C., Balzarolo, M., Barcza, Z., Bernhofer, C., Campbell, C., Cernusca, A., Cescatti, A., Clifton-Brown, J., Dirks, B., Dore, S., Eugster, W., Fuhrer, J., Gimeno, C., Gruenwald, T., Haszpra, L., Hensen, A., Ibrom, A., Jacobs, A., Jones, M., Lanigan, G., Laurila, T., Lohila, A., Manca, G., Marcolla, B., Nagy, Z., Pilegaard, K., Pinter, K., Pio, C., Raschi, A., Rogiers, N., Sanz, M., Stefani, P., Sutton, M., Tuba, Z., Valentini, R., Williams, M., Wohlfahrt, G., 2007. Partitioning european grassland net ecosystem CO_2 exchange into gross primary productivity and ecosystem respiration using light response function analysis. Agric. Ecosyst. Environ. 121, 93–120.
Gond, V., de Pury, D., Veroustraete, F., Ceulemans, R., 1999. Seasonal variations in leaf area index, leaf chlorophyll, and water content; scaling-up to estimate fAPAR and carbon balance in a multilayer, multispecies temperate forest. Tree Physiol. 19, 673–679.
Goudriaan, J., Van Laar, H., 1978. Relations between leaf resistance, CO_2 concentration and CO_2 assimilation in maize, beans, lalang grass and sunflower. Photosyntetica 12, 241–249.
Granier, A., Biron, P., Lemoine, D., 2000a. Water balance, transpiration and canopy conductance in two beech stands. Agric. For. Meteorol. 100, 291–308.
Granier, A., Ceschia, E., Damesin, C., Dufrêne, E., Epron, D., Gross, P., Lebaube, S., Le Dantec, V., Le Goff, N., Lemoine, D., Lucot, E., Ottorini, J., Pontailler, J., Saugier, B., 2000b. The carbon balance of a young beech forest. Funct. Ecol. 14, 312–325.
Granier, A., Reichstein, M., Bréda, N., Janssens, I., Falge, E., Ciais, P., Grünwald, T., Aubinet, M., Berbigier, P., Bernhofer, C., Buchmann, N., Facini, O., Grassi, G., Heinesch, B., Ilvesniemi, H., Keronen, P., Knohl, A., Köstner, B., Lagergren, F., Lindroth, A., Longdoz, B., Loustau, D., Mateus, J., Montagnani, L., Nys, C., Moors, E., Papale, D., Peiffer, M., Pilegaard, K., Pita, G., Pumpanen, J., Rambal, S., Rebmann, C., Rodrigues, A., Seufert, G., Tenhunen, J., Vesala, T., Wang, Q., 2007. Evidence for soil water control on carbon and water dynamics in European forests during the extremely dry year: 2003. Agric. For. Meteorol. 143, 123–145.
Grünwald, T., Bernhofer, C., 2007. A decade of carbon, water and energy flux measurements of an old spruce forest at the Anchor station Tharandt. Tellus 59B, 387–396.
Harrison, R.G., Jones, C.D., Hughes, J.K., 2008. Competing roles of rising CO_2 and climate change in the contemporary European carbon balance. Biogeosciences 5, 1–10.
Hussain, M., Grünwald, T., Tenhunen, J., Li, Y., Mirzae, H., Bernhofer, C., Otieno, D., Dinh, N., Schmidt, M., Wartinger, M., Owen, K., 2011. Summer drought influence on CO_2 and water fluxes of extensively managed grassland in Germany. Agric. Ecosyst. Environ. 141, 67–76.
Jacobs, C.M.J., 1994. Direct impact of atmospheric CO_2 enrichment on regional transpiration. Agricultural University of Wageningen (Ph.D. thesis).
Keenan, T., Baker, I., Barr, A., Ciais, P., Davis, K., Dietze, M., Dragoni, D., Gough, C., Grant, R., Hollinger, D., Hufkens, K., Poulter, B., McCaughey, H., Rackza, B., Ryu, Y., Schaefer, K., Tian, H., Verbeeck, H., Zhao, M., Richardson, A., 2012. Terrestrial biosphere model performance for inter-annual variability of land–atmosphere CO_2 exchange. Global Change Biol. 6, 1971–1987.
Knohl, A., Schulze, E.-D., Kolle, O., Buchmann, N., 2003. Large carbon uptake by an unmanaged 250-year-old deciduous forest in Central Germany. Agric. For. Meteorol. 118, 151–167.
Koster, R., Guo, Z., Dirmeyer, P., Bonan, G., Chan, E., Cox, P., Davies, H., Gordon, C., Kanae, S., Kowalczyk, E., Lawrence, D., Liu, P., Lu, C.-H., Malyshev, S., Mcavaney, B., Mitchell, K., Mocko, D., Oki, T., Oleson, K.W., Pitman, A., Sud, Y., Taylor, C., Verseghy, D., Vasic, R., Xue, Y., Yamada, T., 2006. GLACE: The Global Land–Atmosphere Coupling Experiment. Part i: Overview. J. Hydrometeorol. 7, 590–610.
Kuglitsch, F., Reichstein, M., Beer, C., Carrara, A., Ceulemans, R., Granier, A., Janssens, A., Koestner, B., Lindroth, A., Loustau, D., Matteucci, G., Montagnani, L., Moors,

E., Papale, D., Pilegaard, K., Rambal, S., Rebmann, C., Schulze, E., Seufert, G., Verbeeck, H., Vesala, T., Aubinet, M., Bernhofer, C., Foken, T., Grünwald, T., Heinesch, B., Kutsch, W., Laurila, T., Longdoz, B., Miglietta, F., Sanz, M.J., Valentini, R., 2008. Characterisation of ecosystem water-use efficiency of European forests from eddy covariance measurements. Biogeosci. Discuss. 5, 4481–4519.

Laitat, E., Chermanne, B., Portier, B., 1999. Biomass, carbon and nitrogen allocation in open top chambers under ambient and elevated CO_2 and in a mixed forest stand. A tentative approach for scaling up from the experiments of Vielsalm. In: Ceulemans, R.J.M., Veroustraete, F., Gond, V., Van Rensbergen, J.B.H.F. (Eds.), Forest Ecosystem Modelling, Upscaling and Remote Sensing. Academic Publishing, The Hague, The Netherlands, pp. 33–60.

Lawrence, D., Slater, A., 2008. Incorporating organic soil into a global climate model. Clim. Dyn. 30, 145–160.

Lawrence, D., Thornton, P., Oleson, K., Bonan, G., 2006. The partitioning of evapotranspiration into transpiration, soil evaporation, and canopy evaporation in a GCM: impacts on land–atmosphere interaction. J. Hydrometeorol. 8, 862–880.

Le Dantec, V., Dufrêne, E., Saugier, B., 2000. Interannual and spatial variations of maximum leaf area index in temperate deciduous stands. For. Ecol. Manage. 134, 71–81.

Leuning, R., 1995. A critical appraisal of a combined stomatal-photosynthesis model for C_3 plants. Plant Cell Environ. 18, 339–355.

Ligne, A.D., Heinesch, B., Aubinet, M., 2010. New transfer functions for correcting turbulent water vapour fluxes. Boundary-Layer Meteorol. 137, 205–221.

Mahfouf, J., Noilhan, J., 1991. Comparative study of various formulations of evaporation from bare soil using in situ data. J. Clim. Appl. Meteorol. 30, 1354–1365.

Martin, G., Milton, S., Senior, C., Brooks, M., Ineson, S., Reichler, T., Kim, J., 2010. Analysis and reduction of systematic errors through a seamless approach to modeling weather and climate. J. Clim. 23, 5933–5957.

Meehl, G., Tebaldi, C., 2004. More intense, more frequent, and longer lasting heat waves in the 21st century. Science 305 (994).

Meiresonne, L., Sampson, D., Kowalski, A., Janssens, I., Nadezhdin, N., Cermak, J., Slycken, J.V., Ceulemans, R., 2003. Water flux estimates from a Belgian Scots pine stand: a comparison of different approaches. J. Hydrol. 270, 230–252.

Miralles, D., De Jeu, R., Gash, J., Holmes, T., Dolman, A.J., 2011. Magnitude and variability of land evaporation and its components at the global scale. Hydrol. Earth Syst. Sci. 15, 967–981.

Nagy, Z., Pintér, K., Pavelka, M., Darenová, E., Balogh, J., 2011. Carbon fluxes of surfaces vs. ecosystems: advantages of measuring eddy covariance and soil respiration simultaneously in dry grassland ecosystems. Biogeosciences 8, 2523–2534.

Noilhan, J., Lacarrère, P., 1995. GCM grid-scale evaporation from mesoscale modelling. J. Clim. 8, 206–223.

Noilhan, J., Planton, S., 1989. A simple parametrization of land surface processes for meteorological models. Mon. Wea. Rev. 117, 536–549.

Oleson, K., Lawrence, D., Bonan, G., Flanner, M., Kluzek, E., Lawrence, P., Levis, S., Swenson, S., Thornton, P., 2010. Technical description of version 4.0 of the community land model (CLM), NCAR Technical Note NCAR/TN-478+STR. National Center for Atmospheric Research, April.

Oleson, K., Niu, G.-Y., Yang, Z.-L., Lawrence, D., Thornton, P., Lawrence, P., Stockli, R., Dickinson, R., Bonan, G.B., Levis, S., Dai, A., Qian, T., 2008. Improvements to the Community Land Model and their impact on the hydrological cycle. J. Geophys. Res. 113, 1–26.

Prescher, A.-K., Grünwald, T., Bernhofer, C., 2010. Land use regulates carbon budgets in eastern Germany: from NEE to NBP. Agric. For. Meteorol. 150, 1016–1025.

Rebmann, C., Zeri, M., Lasslop, G., Mund, M., Kolle, O., Schulze, E.-D., Feigenwinter, C., 2010. Treatment and assessment of the CO_2-exchange at a complex forest site in Thuringia, Germany. Agric. For. Meteorol. 150, 684–691.

Reich, P., Kloeppel, B., Ellsworth, D., Walters, M., 1995. Different photosynthesis-nitrogen relations in deciduous hardwood and evergreen coniferous tree species. Oecologia 104, 24–30.

Reichstein, M., Ciais, P., Papale, D., Valentini, R., Running, S., Viovy, N., Cramer, W., Granier, A., Jogée, Allard, V., Aubinet, M., Bernhofer, C., Buchmann, N., Carrara, A., Grünwald, T., Heimann, M., Heinesch, B., Knohl, A., Kutsch, W., Loustau, D., Manca, G., Matteucci, G., Miglietta, F., Ourcival, J.M., Pilegaard, K., Pumpanen, J., Rambal, S., Schaphoff, S., Seufert, G., Soussana, J.-F., Sanz, M.-J., Vesala, M., Zhao, T., 2007. Reduction of ecosystem productivity and respiration during the European summer 2003 climate anomaly: a joint flux tower, remote sensing and modelling analysis. Global Change Biol. 13, 634–651.

Reichstein, M., Falge, E., Baldocchi, D., Papale, D., Valentini, R., Aubinet, M., Berbigier, P., Bernhofer, C., Buchmann, N., Gilmanov, T., Granier, A., Grünwald, T., Havránková, K., Janous, D., Knohl, A., Laurela, T., Lohila, A., Loustau, D., Matteucci, G., Meyers, T., Miglietta, F., Ourcival, J.-M., Rambal, S., Rotenberg, E., Sanz, M., Tenhunen, J., Seufert, G., Vaccari, F., Vesala, T., Yakir, D., 2005. Phase and amplitude of ecosystem carbon release and uptake potentials as derived from FLUXNET measurements. Global Change Biol. 11, 1424–1439.

Reichstein, M., Tenhunen, J., Roupsard, O., Ourcival, J.-M., Rambal, S., Miglietta, F., Peressotti, A., Pecchiaris, M., Tirone, G., Valentini, R., 2002. Severe drought effects on ecosystem CO_2 and H_2O fluxes at three Mediterranean evergreen sites: revision of current hypotheses? Global Change Biol. 8, 999–1017.

Rivalland, V., Calvet, J.-C., Berbigier, P., Granier, Y.B.A., 2005. Transpiration and CO_2 fluxes of a pine forest: modelling the undergrowth effect. Annales Geophysicae 23, 291–304.

Schär, C., Lüthi, D., Beyerle, U., Heise, E., 1999. The soil-precipitation feedback: a process study with a regional climate model. J. Clim. 12, 722–741.

Schär, C., Vidale, P., Lüthi, D., Frei, C., Häberli, C., Liniger, M., Appenzeller, C., 2004. The role of increasing temperature variability in European summer heatwaves. Nature 427, 332–336.

Sellers, P., Randall, D., Collatz, G., Berry, J., Field, C., Dazlich, D., Zhang, C., Colleleo, G., Bounoua, L., 1996. A revised parameterization (SiB2) for atmospheric GCMs. Part I: Model formulation. J. Clim. 9, 676–705.

Seneviratne, S., Lüthi, D., Litschi, M., Schär, C., 2006. Land–atmosphere coupling and climate change in Europe. Nature 443 (14), 205–209.

Sutanto, S., Wenninger, J., Coenders-Gerrits, A., Uhlenbrook, S., 2012. Partitioning of evaporation into transpiration, soil evaporation and interception: a combination of hydrometric measurements and stable isotope analyses. Hydrol. Earth Syst. Sci. Discuss. 9, 3657–3690.

Tallaksen, L., 1991. Recession rate and variability with special emphasis upon the influence of evapotranspiration. Rapportserie: Hydrologi Nr. 25. Universitetet i Oslo.

Teuling, A., Hirschi, H., Ohmura, A., Wild, M., Reichstein, M., Ciais, P., Buchmann, N., Ammann, C., Montagnani, L., Richardson, A., Wohlfahrt, G., 2009. A regional perspective on trends in continental evaporation. Geophys. Res. Lett. 36, 1–5.

Thompson, S., Harman, C., Heine, P., Katul, G., 2010. Vegetation-infiltration relationships across climatic and soil type gradients. J. Geophys. Res. 115, 1–12.

Tolk, L., Peters, W., Meesters, A., Groenendijk, M., Vermeulen, A., Steeneveld, G., Dolman, A., 2009. Modelling regional scale surface fluxes, meteorology and CO_2 mixing ratios for the Cabauw tower in the Netherlands. Biogeosciences 6, 2265–2280.

Twine, T.E., Kustas, W.P., Norman, J.M., Cook, D.R., Houser, P.R., Meyers, T.P., Prueger, J.H., Starks, P.J., Wesley, M.L., 2000. Correcting Eddy-covariance flux underestimates over a grassland. Agric. For. Meteorol. 103, 279–300.

Van den Hoof, C., Hanert, E., Vidale, P., 2011. Simulating dynamic crop growth with an adapted land surface model – JULES-SUCROS: model development and validation. Agric. For. Meteorol. 151, 137–153.

van Genuchten, M., 1980. A closed-form equation for predicting the hydraulic conductivity of unsaturated soils. Soil Sci. Soc. Am. J. 44, 892–898.

Verseghy, D., Lazare, M., McFarlane, N., 1993. Class – a Canadian land surface scheme for GSMS, II. vegetation model and coupled runs. Int. J. Climatol. 13, 111–133.

Verstraeten, W., Muys, B., Feyen, J., Veroustraete, F., Minnaert, M., Meiresonne, L., De Schrijve, A., 2005. Comparative analysis of the actual evapotranspiration of Flemish forest and cropland, using the soil water balance model WAVE. HESS 9 (3).

Walters, D., Best, M., Bushell, A., Copsey, D., Edwards, J., Falloon, P., Harris, C., Lock, A., Manners, J., Morcrette, C., Roberts, M., Stratton, R., Webster, S., Wilkinson, J., Willett, M., Boutle, I., Earnshaw, P., Hill, P., MacLachlan, C., Martin, G., Moufouma-Okia, W., Palmer, M., Rooney, J.P.G., Scaife, A., Williams, K.D., 2011. The Met Office Unified Model Global Atmosphere 3.0/3.1 and JULES Global Land 3.0/3.1 configuration. Geosci. Model Dev. 4, 919–941.

Wilson, K., Goldstein, A., Falge, E., Aubinet, M., Baldocchi, D., Berbigier, P., Bernhofer, C., Ceulemans, R., Dolman, H., C. Field, A.G., Ibrom, A., Law, B., Kowalski, A., Meyers, T., Moncrieff, J., Monson, R., Oechal, W., Tenhunen, J., Valentini, R., Verma, S., 2002. Energy balance closure at FLUXNET sites. Agric. For. Meteorol. 113, 223–243.

Wilson, K., Hanson, P., Mulholland, P., Baldocchi, D., Wullschleger, S., 2001. A comparison of methods for determining forest evapotranspiration and its components: sap-flow, soil water budget, eddy covariance and catchment water balance. Agric. For. Meteorol. 106, 153–168.

Wong, S., Cowan, I., Farquhar, G., 1979. Stomatal conductance correlates with photosynthetic capacity. Nature 282, 287–305.

Wösten, J., Lilly, A., Nemes, A., Le Bas, C., 1999. Development and use of a database of hydraulic properties of European soils. Geoderma 90, 169–185.

Wullschleger, S.D., 1993. Biochemical limitations to carbon assimilation in C_3 plants – a retrospective analysis of the A/Ci curves from 109 species. J. Exp. Bot. 44, 907–920.

Zaitchik, B., MacAlady, A., Bonneau, L., Smith, R., 2006. Europe's 2003 heat wave: a satellite view of impacts and land–atmosphere feedbacks. Int. J. Climatol. 26, 743–769.